A Comparison of Radial Diffusion Coefficients in 1-D and 3-D Long-Term Radiation Belt Simulations

A. Y. Drozdov[1*], H. J. Allison[2], Y. Y. Shprits[1,2,3], S.R. Elkington[4], N.A. Aseev[2,3]

[1]University of California Los Angeles, CA, USA
[2]GFZ German Centre for Geosciences, Potsdam, Germany
[3]Institute of Physics and Astronomy, University of Potsdam, Germany
[4]Laboratory for Atmospheric and Space Physics, University of Colorado Boulder, Boulder, Colorado, USA

Key Points:

- Simulations using different radial diffusion coefficients, except Ali et al. (2016), produce similar results
- Using Ali et al. (2016), D_{LL} yields flux values significantly lower than observations
- 1.04 MeV electron flux simulated with Brautigam and Albert (2000) D_{LL} shows the best agreement with observations

*UCLA

Corresponding author: A. Drozdov, adrozdov@ucla.edu

Abstract

Radial diffusion is one of the dominant physical mechanisms driving acceleration and loss of radiation belt electrons. A number of parameterizations for radial diffusion coefficients have been developed, each differing in the dataset used. Here, we investigate the performance of different parameterizations by Brautigam and Albert (2000), Brautigam et al. (2005), Ozeke et al. (2014), Ali et al. (2015, 2016); Ali (2016), and Liu et al. (2016) on long-term radiation belt modeling using the Versatile Electron Radiation Belt (VERB) code, and compare the results to Van Allen Probes observations. First, 1-D radial diffusion simulations are performed, isolating the contribution of solely radial diffusion. We then take into account effects of local acceleration and loss showing additional 3-D simulations, including diffusion across pitch-angle and energy, as well as mixed diffusion. For the L* range studied, the difference between simulations with Brautigam and Albert (2000), Ozeke et al. (2014), and Liu et al. (2016) parameterizations is shown to be small, with Brautigam and Albert (2000) offering the best agreement with observations. Using Ali et al. (2016)'s parameterization tended to result in a lower flux at 1 MeV than both the observations and the VERB simulations using the other coefficients. We find that the 3-D simulations are less sensitive to the radial diffusion coefficient chosen than the 1-D simulations, suggesting that for 3-D radiation belt models, a similar result is likely to be achieved, regardless of whether Brautigam and Albert (2000), Ozeke et al. (2014), and Liu et al. (2016) parameterizations are used.

1 Introduction

Fluctuations in the magnetic and electric fields result in diffusive motion of radiation belt electrons across Roederer's L* parameter (Roederer, 1970; Flthammar, 1965), a version of the third adiabatic invariant. L* diffusion (henceforth referred to as radial diffusion) occurs at constant first and second adiabatic invariant, and the electron's energy is increased (reduced) with diffusion into regions of stronger (weaker) magnetic field. Much of the dynamics of the radiation belts can be attributed to radial diffusion and the subsequent energy change of the electron populations (Shprits et al., 2008), and so understanding the rate of the diffusion is a vital factor for accurately predicting and reconstructing the evolution of electron populations.

The primary origin of electric and magnetic fluctuations, driving radial diffusion, is widely accepted to be ultra-low frequency (ULF) wave activity (Elkington et al., 1999) in the Pc-5 band (1.67 mHz - 6.67 mHz (Jacobs et al., 1964)). Wave-particle interactions between these ULF waves and radiation belt electrons are particularly effective when the wave frequency is a multiple of the electron drift frequency, constituting a drift-resonant interaction. If interactions with Pc-5 waves continue over a broad frequency range, then the displacement of a particle in L* may evolve stochastically, following continuous interactions with multiple waves, and be described as a diffusive process (Ukhorskiy et al., 2009; Ukhorskiy & Sitnov, 2013). In this diffusive regime, the radial diffusion coefficient, D_{LL}, quantifies the mean square displacement of electrons across L*, and is a measure of the radial diffusion rate.

Analytic expressions quantifying rates of radial diffusion can be derived starting with either the drift equations, describing the influence of the perturbing waves (Flthammar, 1965; Fälthammar, 1968; Schulz & Eviatar, 1969; Schulz & Lanzerotti, 1974; Ukhorskiy et al., 2005), or starting from a Hamiltonian formulation (Brizard & Chan, 2001). The relevant form of the diffusion coefficient will depend on whether the waves are electromagnetic in nature, potentially resulting from Alfvenic fluctuations in the magnetosphere, or whether the wave can be ascribed to electrostatic variations in a large-scale potential field (Cornwall, 1968). If the field variations are described in terms of an electrostatic

potential, the diffusion coefficient for particles drifting with frequency ω_d takes the form

$$D_{LL}^{ES} = \frac{1}{8B_E^2 R_E^2} L^6 \sum_m P_m^E (L, m\omega_d). \quad (1)$$

Here B_E and R_E are the Earth's dipole moment and radius, respectively, and P_m^E is the power spectral density of the perturbing electric fields at the resonant frequency $m\omega_d$, where m describes the global azimuthal structure of the waves. Variations in the dawn-dusk electric field associated with global magnetospheric convection is one example of such field perturbations (Cornwall, 1968). On the other hand, if the perturbation is magnetic in nature, where magnetic and electric perturbations are related by Faraday's law, then the diffusion can be described by the expression

$$D_{LL}^{M} = \frac{\mu^2}{8q^2\gamma^2 B_E^2 R_E^4} L^4 \sum_m m^2 P_m^B (L, m\omega_d). \quad (2)$$

In this expression, γ is the Lorentz factor, μ the relativistic first adiabatic invariant, and P_m^B is the power spectral density of the compressional wave magnetic field at frequency $m\omega_d$. The electrostatic diffusion coefficient (1) has an L^6 dependence, plus the L dependence in P_m^E. The L dependence of the electromagnetic diffusion coefficient is more complicated since γ also depends on L. In the ultra-relativistic limit $\gamma^2 \propto L^{-3}$, so for radiation belt electrons L^4/γ^2 is approximately proportional to L^7, not including the L dependence implicit in P_m^B (Elkington et al., 2003).

We note that in the classic "electromagnetic" diffusion formulas given by Flthammar (1965) the particle perturbations leading to diffusion result from two effects: variations in the magnetic field along the drift orbit, as well as the electric field induced by these magnetic field fluctuations. That is, the particle motion is a result of the Faraday-coupled electric and magnetic field variations along a trajectory. In practice, however, it is difficult to distinguish between the electrostatic variations implied in Equation (1) from the induced electric fields measured in space, leading to the Fei et al. (2006) expression in Equation (2). Perry et al. (2005) showed that the magnetic field phase and the induced electric field phase are not independent. The Faraday-coupled fields, including correct phase, will generally lead to reduced rates of radial diffusion from that given in Equations (2) and (1).

A number of studies have calculated D_{LL} coefficients based on the power spectral density (PSD) of ULF waves (e.g., Brautigam & Albert, 2000; Ozeke et al., 2012, 2014; Liu et al., 2016; Ali et al., 2016, 2015; Lejosne et al., 2013; Olifer et al., 2019; Barani et al., 2019), using different data sets and formulations. Several options for D_{LL} coefficients are therefore available. However, a full comparison of how well each available D_{LL} parameterization performs in a diffusion model, both in respect to observations, and to the results from other D_{LL} coefficients, has yet to be determined. This paper is an extension of a previous study (Drozdov et al., 2017) in which the sensitivity of long-term simulations, performed with the Versatile Electron Radiation Belt (VERB) code, to both the Brautigam and Albert (2000) and Ozeke et al. (2014) radial diffusion coefficients (D_{LL}), was investigated. Here we consider more recent parameterizations of D_{LL} (Ali et al., 2015, 2016; Liu et al., 2016) and an additional D_{LL} by Brautigam et al. (2005), contrasting the results achieved using these parameterizations to the widely used Brautigam and Albert (2000) and Ozeke et al. (2014) diffusion coefficients.

1.1 Parameterizations of radial diffusion coefficients

The radial diffusion coefficients given by Brautigam and Albert (2000) consist of both an electromagnetic and electrostatic term (denoted here as D_{LL}^{BAEM} and D_{LL}^{BAES}, respectively), following the formalism presented by Flthammar (1965). A month of in-situ measurements at L = 6.6 (Lanzerotti & Morgan, 1973) and 18 days of ground magnetometer measurements at L = 4 (Lanzerotti & Morgan, 1973) were used to construct

a Kp parameterized D_{LL}^{BAEM} coefficient. Brautigam and Albert (2000) then calculated the electrostatic D_{LL}^{BAES} term following Cornwall (1968), as a linear function of Kp. Both D_{LL}^{BAEM} and D_{LL}^{BAES} are explicitly defined for the Kp range $1 \leq \text{Kp} \leq 6$. Subsequent work has demonstrated that using D_{LL}^{BAES} alongside D_{LL}^{BAEM} in radiation belt models results in an over-estimation of the electron content in the slot region (Kim et al., 2011; Ozeke et al., 2012). We therefore follow the standard convention here (e.g., Glauert et al., 2014) and exclude D_{LL}^{BAES} from this study, using only the electromagnetic component

$$D_{LL}^{BA} \equiv D_{LL}^{BAEM}, \tag{3}$$

where

$$D_{LL}^{BAEM} = L^{10} \cdot 10^{0.506Kp - 9.325} \tag{4}$$

in units of day^{-1}.

Ozeke et al. (2014), following the work by Fei et al. (2006), separated the radial diffusion coefficients into two terms; one accounting for the azimuthal electric field D_{LL}^{OE} of the ULF waves and the other for the waves' compressional magnetic field D_{LL}^{OM}. Collectively, they provide the D_{LL}^{O} coefficient:

$$D_{LL}^{O} = D_{LL}^{OM} + D_{LL}^{OE}. \tag{5}$$

In recent studies, there has been some discussion as to whether it is valid to assume that the azimuthal electric field and the compressional magnetic field are uncorrelated (Lejosne et al., 2013; Lejosne & Kollmann, 2019), a necessary assumption to treat D_{LL}^{OE} and D_{LL}^{OM} separately in the manner shown. However, we do not consider this question further here, but rather focus on how well the Ozeke et al. (2014) D_{LL} is able to reproduce observations. Both the D_{LL}^{OM} and D_{LL}^{OE} are parameterized by the Kp activity index. The azimuthal electric field PSD values used to determine the Kp parameterization of the D_{LL}^{OE} coefficient were given by >15 years of ground magnetometer measurements at 7 different L shells, and the resulting expression for the electric D_{LL}^{OE} coefficient is

$$D_{LL}^{OE} = L^{8} \cdot 6.62 \cdot 10^{-13} \cdot 10^{-0.0327L^2 + 0.625L - 0.0108Kp^2 + 0.499Kp} \tag{6}$$

in units of day^{-1}. The compressional magnetic field component parameterization was determined from GOES, AMPTE, and THEMIS satellite measurements and is given as

$$D_{LL}^{OM} = L^{6} \cdot 2.6 \cdot 10^{-8} \cdot 10^{0.217L + 0.461Kp} \tag{7}$$

again, in units of day^{-1}. Similar to the Brautigam and Albert (2000) radial diffusion coefficients, the Ozeke et al. (2014) coefficients are also determined for $\text{Kp} \leq 6$.

More recently, Ali et al. (2016) also used the approach of separating the radial diffusion coefficient into terms for both the ULF wave azimuthal electric field and the compressional magnetic field (Fei et al., 2006; Brizard & Chan, 2001)

$$D_{LL}^{A} \equiv D_{LL}^{AM} + D_{LL}^{AE}. \tag{8}$$

The diffusion coefficients given by Ali et al. (2016) were determined using three years of the Van Allen Probe data set, utilizing the Electric Fields and Waves (EFW) instrument and the Electric and Magnetic Field Instrument Suite (EMFISIS) to take in-situ observations of both the electric field and compressional magnetic field. The Kp index was again used to parameterize the magnetic D_{LL}^{AM} and electric D_{LL}^{AE} coefficients, and the resulting expressions were

$$D_{LL}^{AM} = \exp(-16.253 + 0.225 \cdot Kp \cdot L^{*} + L^{*}) \tag{9}$$

and

$$D_{LL}^{AE} = \exp(-16.951 + 0.181 \cdot Kp \cdot L^{*} + 1.982 \cdot L^{*}) \tag{10}$$

both in given units of days^{-1} and valid for $0 \leq \text{Kp} \leq 5$. Notice that, while the Brautigam and Albert (2000) and Ozeke et al. (2014) parameterizations are in terms of L, the McIlwain L value (McIlwain, 1961), D_{LL}^{A} is explicitly given in terms of L*.

Previously, Ali et al. (2015) constructed a parameterization for the magnetic component of the radial diffusion coefficient using observations from the magnetometer on board the Combined Release and Radiation Effects Satellite (CRRES). The authors analyzed magnetic wave power and derived a fit of the magnetic diffusion coefficient as a Gaussian function plus a power law function (Ali et al., 2015, eq. 15). The coefficients for this fit were provided in a form of lookup-table for different levels of geomagnetic activity. In his postdoctoral thesis, Ali (2016) continued the construction of D_{LL}^{M} as a function of L, Kp and μ based on the same data set as in (Ali et al., 2015), resulting in:

$$D_{LL}^{AM(CRRES)} = \exp(-16.618 + 0.00060104 \cdot \mu + 0.10003 \cdot Kp \cdot L + L) \tag{11}$$

where the units of $D_{LL}^{AM(CRRES)}$ and μ are days^{-1} and MeV/G respectively. Equation (11) is applicable for $4.0 \leq L \leq 6.5$, $1 \leq Kp \leq 7$, $500 \leq \mu \leq 5000$ MeV/G and is similar to equation (9); however, it provides explicit dependence on μ and is based on observations taken during the previous solar cycle.

Assuming a purely electrostatic field, a parameterization of the electrostatic component of the radial diffusion coefficient based on CRRES measurements was given by Brautigam et al. (2005). In their study, the Electric Field Instrument (EFI) on board CRRES was used to derive a fit of electric field power spectral as a function L, Kp, and frequency. Based on the formalism presented by Flthammar (1965), the radial diffusion coefficient can be written as

$$D_{LL}^{E} = \frac{P(f_d, L, Kp)}{8 \cdot R_E^2 \cdot B_{eq}^2} \tag{12}$$

where P is an electric power spectral density, f_d is drift frequency, R_E is the Earth radius, and B_{eq} is equatorial magnetic field at the corresponding L. Using the representation of the azimuthal component of the global electric field from Holzworth and Mozer (1979), Brautigam et al. (2005) derived an expression for P:

$$P(f_d, L, Kp) = a \cdot L^b \cdot \exp(c \cdot Kp) \tag{13}$$

where P is given in units of $(\text{mV/m})^2/\text{mHz}$, and coefficients a, b and c are given in a form of lookup table for different values of the drift frequency f_d (Brautigam et al., 2005, table 3). Following the drift frequency f_d (in mHz) equation provided by Brautigam et al. (2005), we assume a dipole magnetic field model and substitute for constants to obtain the drift frequency formula:

$$f_d = \frac{0.1183 \cdot \mu}{\sqrt{L^4 + 1.2133 \cdot L + \cdot \mu}} \tag{14}$$

where μ is in units of MeV/G. The electrostatic component of radial diffusion coefficient, $D_{LL}^{BE(CRRES)}$, is then given as

$$D_{LL}^{BE(CRRES)} = 2.7818 \cdot 10^{-4} \cdot L^6 \cdot P(f_d, L, Kp) \tag{15}$$

where $D_{LL}^{BE(CRRES)}$ is in units of days^{-1}, P has units of $(\text{mV/m})^2/\text{mHz}$ from equation (13), and f_d is in mHz from equation (14).

The final radial diffusion coefficient considered in this study is that given by Liu et al. (2016). Unlike the studies discussed above (e.g., Brautigam & Albert, 2000; Ozeke et al., 2014; Ali et al., 2016), Liu et al. (2016) determine only the electric field component from the Fei et al. (2006) approach, arguing that, since the electric component is greater than the magnetic by orders of magnitude, radial diffusion is primarily controlled

by the electric component of the ULF wave. A similar argument was also discussed by Ozeke et al. (2014) and Ali et al. (2016).

$$D_{LL}^{L} \equiv D_{LL}^{LE}. \tag{16}$$

Seven years of measurements from the THEMIS satellites were used to determine a Kp and μ-dependent expression for D_{LL}^{LE}. Previously, Ozeke et al. (2014) and Ali et al. (2016) had not identified a μ dependence in the D_{LL}^{LE} coefficient. Brautigam and Albert (2000) did include a μ dependence in the electrostatic radial diffusion coefficient; however, the convention to omit D_{LL}^{BAES} and use only D_{LL}^{BAEM} for the Brautigam and Albert (2000) parameterization means that, in this study, only the coefficients provided by Liu et al. (2016), Ali (2016) and Brautigam et al. (2005) vary with particle energy and pitch angle. Using the THEMIS data, Liu et al. (2016) found that D_{LL}^{LE} can be expressed as

$$D_{LL}^{LE} = 1.115 \cdot 10^{-6} \cdot 10^{0.281 \cdot Kp} \cdot L^{8.184} \cdot \mu^{-0.608} \tag{17}$$

in units of day^{-1}.

1.2 Various assumptions for derived radial diffusion coefficients

When considering the variety of the available radial diffusion coefficients, it is worth paying special attention to the assumptions made and the coverage and quality of data used, for their evaluation. The measurements used by Brautigam and Albert (2000) are very limited, both spatially and temporally. The continuous function for the electromagnetic coefficient extending over $L = 3{-}6.6$ is constructed based on measurements from two locations: $L = 4$ and $L = 6.6$. As mentioned in section 1.1, their data set duration does not exceed one month. Both Brautigam et al. (2005) and Ali et al. (2016) use several months of CRRES observations. Brautigam et al. (2005) considered the period from January through October 1991, while Ali et al. (2016) utilized a year of measurements, extending from October 1990 until October 1991.

Ozeke et al. (2014) used the longest and most extensive data set. The ground-based measurements included CARISMA (Canadian Array for Real-time Investigations of Magnetic Activity) observations from January 1990 to May 2005, and SAMNET (Sub-Auroral Magnetometer NETwork) observations from 1987 to 2002. These observations involved mapping ULF wave power observed on the ground to a corresponding electric field in space, making a number of assumptions about the spatial structure of the waves and the characterize all fluctuations observed on the ground as guided Alfven waves in a pure dipole. In situ satellite measurements used by Ozeke et al. (2014) included GOES observations from 1996 to 2005 and measurements from 5 THEMIS (Time History of Events and Macroscale Interactions during Substorms) spacecraft in the range L=5-7 from 2007 to 2011. The authors also indirectly included measurements from AMPTE (Active Magnetospheric Particle Tracers Explorers) by using the figure of power spectral density presented by Takahashi and Anderson (1992). Liu et al. (2016) used only one set of THEMIS-D satellite measurements covering a period from January 2008 to December 2014. Ali et al. (2016) used the measurements from Van Allen Probes from September 2012 to August 2015.

Observational platforms can themselves influence the calculated power spectral density. As noted in Ozeke et al. (2014), the high apogee of the THEMIS spacecraft leads to extreme Doppler effects in the inner magnetosphere, causing an over-estimation of the power spectral densities at low-L. For this reason, Ozeke et al. (2014) only considered THEMIS measurements in the L=5-7 range in the validation of their method. THEMIS also suffers from "shorting effects" as it moves into the plasmasphere, causing large DC offsets that can potentially pollute the power spectral density in the inner magnetosphere unless properly accounted for and removed (Califf & Cully, 2016). Similarly, DC offsets are often observed on THEMIS (which may be attributable to photoelectrons) that vary

with spacecraft position; these shifting errors may also contribute to an overestimation of observed power at ULF frequencies (Califf et al., 2014). Additionally, rotational eclipses on THEMIS at dawn and dusk make observations of the azimuthal electric field at these local times difficult, and the lack of information along the THEMIS spin axis affects measurements when the local magnetic field differs from the mean field aligned system (Malaspina et al., 2015) can similarly cause significant errors in THEMIS-estimated electric fields used by Liu et al. (2016) if these effects had not properly accounted for.

In the work of Ozeke et al. (2014) assumptions are made regarding the azimuthal spatial structure of the wave activity, resulting in a potential factor of 4 difference in the power spectral density mapped from the ground into space. Of particular concern may be the misidentification of Alfvenic waves driven by drift-bounce (Ozeke & Mann, 2001; Mager & Klimushkin, 2005) and other plasma instabilities, which will cause overestimation of the power spectral density causing diffusion.

Finally, single-point measurements, of necessity, require some assumptions about the azimuthal mode structure of the observed waves. For the D_{LL} estimates provided in all the works under examination here, an $m = 1$ assumption is uniformly made. However, modeling (Elkington et al., 2012; Tu et al., 2012; Li et al., 2017) and observational (Sarris et al., 2013; Barani et al., 2019) studies indicate that significant power may be attributable to larger azimuthal m numbers, causing an overestimation of the power in the $m = 1$ mode.

1.3 Comparison of the radial diffusion coefficients

Figure 1 shows a comparison between different radial diffusion coefficients. Two values of Kp are considered: Kp = 1 for low activity (left panel) and Kp = 5 for active conditions (right panel). For the Ali (2016) and Brautigam et al. (2005) coefficients, a range of μ values are shown, $\mu \in [500; 5000]$ MeV/G, signified by shaded areas. For the Liu et al. (2016) coefficient, the range is $\mu \in [400; 8000]$ MeV/G. The range of μ shown is either explicitly prescribed by the model or corresponds to the respective study. Sudden changes in the Brautigam et al. (2005) coefficient at $L \approx 4.2$ are due to the use of the lookup table in equation (13).

At both levels of activity, the Ozeke et al. (2014) D_{LL}^{OM}, Ali et al. (2016) D_{LL}^{AM} and Ali (2016) $D_{LL}^{AM(CRRES)}$ are considerably lower than the D_{LL}^{E} coefficients, indicating that the rate of radial diffusion is primarily governed by the azimuthal electric fields when considered in the Fei et al. (2006) approach. As mentioned above, this observation has been discussed in a number of studies (e.g., Ozeke et al., 2014; Ali et al., 2015, 2016; Li et al., 2016a) and is the justification for Liu et al. (2016) omitting the magnetic diffusion coefficient altogether. Brautigam and Albert (2000) D_{LL}^{BA}, Brautigam et al. (2005) $D_{LL}^{BE(CRRES)}$, Ozeke et al. (2014) D_{LL}^{O}, and Liu et al. (2016) D_{LL}^{L} are in close agreement for L = 3 - 5.5 at Kp = 1. However, at Kp = 5, while D_{LL}^{BA} and D_{LL}^{O} are still comparable, D_{LL}^{L} and $D_{LL}^{BE(CRRES)}$ have not increased as readily. The D_{LL}^{L} and $D_{LL}^{BE(CRRES)}$ coefficients increase with decreasing μ, suggesting that lower energy electrons undergo faster radial diffusion. At Kp = 1, the D_{LL}^{L} values for $\mu = 400$ MeV/G are the largest of all shown, but for Kp = 5, D_{LL}^{L} is less than D_{LL}^{BA} and D_{LL}^{O} over all L and μ. The magnetic radial diffusion coefficient of Ali (2016), $D_{LL}^{AM(CRRES)}$, increases with increasing μ. However, the largest values of the magnetic diffusion coefficient are still lower than the electric diffusion coefficients, given the limits of the model's fit domain ($\mu \leq 5000$ MeV/G).

While a comparison of D_{LL} values is instructive, a better test of the different parameterizations is use in a radiation belt model followed by comparison with observations. In this study, we use the parameterizations of radial diffusion described above in

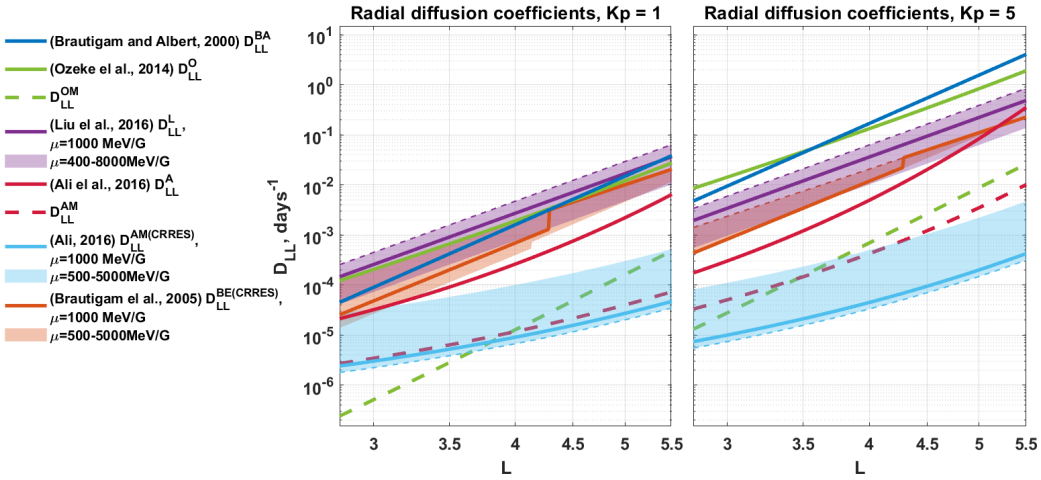

Figure 1. A comparison of various radial diffusion coefficients. We show the electromagnetic D_{LL} from Brautigam and Albert (2000) (dark blue line); magnetic D_{LL} from Ozeke et al. (2014) (green dashed); electric D_{LL} from Ozeke et al. (2014) (green solid line); electric D_{LL} at $\mu = 1000$ MeV/G from Liu et al. (2016) (solid magenta line), as well as the variation of this coefficient for $\mu \in [400, 8000]$ (magenta area); electric D_{LL} from Ali et al. (2016) (red solid line); magnetic D_{LL} from Ali et al. (2016) (red dashed line); magnetic D_{LL} at $\mu = 1000$ MeV/G from Ali (2016) (cyan line), as well as the variation of this coefficient for $\mu \in [500, 5000]$ MeV/G (cyan area); electric D_{LL} at $\mu = 1000$ MeV/G from Brautigam et al. (2005) (orange line), as well as the variation of this coefficient for $\mu \in [500, 5000]$ MeV/G (orange area). When a μ range is given, dashed lines indicate left (lower) boundary of μ range. Left panel corresponds to Kp=1 and right panel to Kp=5.

long-term runs of the VERB model and compare results with Van Allen Probe observations. This approach is described in detail in the following sections.

2 Methodology

2.1 Data

A period nearly from the start of the Van Allen Probes mission (Stratton et al., 2013), spanning from October 1, 2012 to October 1, 2013, has been considered for the study.

Initial and boundary conditions for the VERB model runs are formed from measurements from Van Allen Probe satellites RBSP-A and RBSP-B, using both the Relativistic Electron Proton Telescope (REPT: Baker et al., 2013) and the Magnetic Electron Ion Spectrometer (MagEIS: Blake et al., 2013) instruments. MagEIS measurements are used for <1.8 MeV and REPT for energies ≥1.8 MeV. The twin Van Allen Probes have an orbital period of approximately 9 hours, regularly sampling $L^* \approx 1.2 - 5.5$. Across MagEIS and REPT, electron energies from ∼30 keV to $>\sim$ 8 MeV can be measured, and the spinning satellite is capable of sampling several pitch angle sectors. To formulate the data-driven boundaries, the measured flux values were binned into 1-day bins, and into L^* bins ranging from $L^* = 1$ - 5.5 in steps of 0.1 L^*. The electron flux is linearly interpolated onto an equatorial pitch angle grid, in steps of 5^o, from 0^o to 90^o.

For comparisons of the model output with observations, measurements of ~ 1 MeV electrons from the MagEIS detector at an equatorial pitch angle (α_{eq}) of 70^o are used. All equatorial pitch angles and L^* values are calculated with the TS07D magnetic field model (Tsyganenko & Sitnov, 2007).

2.2 VERB code

The evolution of electron phase space density in the radiation belts is described by the Fokker-Planck equation (Schulz & Lanzerotti, 1974) in terms of L^*, energy, and equatorial pitch angle. Using a single grid approach, the VERB code (Subbotin & Shprits, 2009, 2012; Shprits et al., 2015) computes a numerical solution of the equation:

$$\frac{\partial f}{\partial t} = \frac{1}{G}\frac{\partial}{\partial L^*}\bigg|_{V,K} G\left\langle D_{L^*L^*}\right\rangle \frac{\partial f}{\partial L^*}\bigg|_{V,K} +$$
$$\frac{1}{G}\frac{\partial}{\partial V}\bigg|_{L^*,K} G\left(\left\langle D_{VV}\right\rangle \frac{\partial f}{\partial V}\bigg|_{L^*,K} + \left\langle D_{VK}\right\rangle \frac{\partial f}{\partial K}\bigg|_{L^*,V}\right) +$$
$$\frac{1}{G}\frac{\partial}{\partial K}\bigg|_{L^*,V} G\left(\left\langle D_{KK}\right\rangle \frac{\partial f}{\partial K}\bigg|_{L^*,V} + \left\langle D_{VK}\right\rangle \frac{\partial f}{\partial V}\bigg|_{L^*,K}\right) - \frac{f}{\tau_{lc}} \tag{18}$$

where V is adiabatic invariant, $V \equiv \mu \cdot (K+0.5)^2$ and $G = -2\pi B_0 R_E^2\sqrt{8\mu \cdot m_0}/(K+0.5)^2/L^{*2}$ is the Jacobian of the transformation from an adiabatic invariant system (μ, J, Φ), B_0 is the field on the equator of the Earths surface, m_0 is the electron's rest mass. Bounce-averaged diffusion coefficients are denoted by $\left\langle D_{L^*L^*}\right\rangle, \left\langle D_{VV}\right\rangle, \left\langle D_{KK}\right\rangle$ and $\left\langle D_{VK}\right\rangle$. A loss term of f/τ_{lc} is included to incorporate losses to the atmosphere and magnetopause, where τ_{lc} represents the electron‘s lifetime inside the loss cone or outside of the last closed drift shell. The region of outer boundary loss is estimated from the Shue et al. (1998) magnetopause location.

V and K are convenient for numerical calculations, because K is independent of particle energy, and V depends only weakly on particle pitch angle. We used the Full Diffusion Code (FDC) (Ni et al., 2008; Shprits & Ni, 2009; Orlova & Shprits, 2011) to compute bounce-averaged diffusion coefficients in the manner described in previous work by Drozdov et al. (2017). Plasmaspheric hiss is included inside the plasmapause using the wave model by Orlova et al. (2014), chorus waves are included on the day and night sides Orlova et al. (2012), and VLF transmitters and lightning generated whistlers are included as described by Subbotin et al. (2011). All diffusion coefficients, corresponding to local scattering as well as radial diffusion, are dependent on the Kp-index. The radial diffusion parameterizations are all also Kp-dependent and are assumed to follow the described Kp trend for all values of Kp.

The 3-d VERB code simulation domain extends from $L^* = 1$ to $L^* = 5.5$, and encompasses electron energies from 10 keV to 10 MeV at $L^* = 5.5$. Equatorial pitch angles from 0.7^o to 89.3^o are covered, and the grid in the L^*, V, K space has dimensions of $46 \times 100 \times 101$. To define the calculation box, boundary conditions are required at the minimum and maximum values of these three variables. For the inner L^* boundary, at $L^* = 1$, the phase space density is zero, capturing total loss to the atmosphere. The outer L^* is set from the Van Allen Probes data, as described in section 2.1, and is updated for each day of the run. The Van Allen Probes flux is converted to phase space density and the logarithm of the phase space density interpolated to the V and K simulation grid. However, Van Allen Probes measurements do not cover the full range of V and K. To cover V and K values not observed by the Van Allen Probes, we create a synthetic phase space density array. We calculate a synthetic phase space density assuming the sin pitch angle distribution and the average energy spectra. We normalize this array to a valid measurement as close as possible to 1 MeV, $\alpha_{eq} = 90^o$. Thus, two 2D arrays are created: the interpolated phase space density from the Van Allen Probe observations and the synthetic normalized phase space density array. All data gaps in

the first array are replaced with the values from the second, and any remaining data gaps set to zero. The initial condition is created from the Van Allen Probes data in a similar fashion, but for each L^* bin rather than for each time bin using steady state solution for the synthetic array. All 365 2-D slices of the outer boundary condition and each L^* slice of the initial condition are visually inspected for interpolation artifacts.

The VERB code is used for both 1-D (VERB-1D) and 3-D (VERB-3D) simulations. In the case of the 1-D simulation, where energy and pitch angle diffusion are omitted, equation (18) simplifies to:

$$\frac{\partial f}{\partial t} = \frac{1}{G}\frac{\partial}{\partial L^*}\bigg|_{V,K} G\left\langle D_{L^*L^*}\right\rangle \frac{\partial f}{\partial L^*}\bigg|_{V,K} - \frac{f}{\tau} \tag{19}$$

where τ has been modified to now be the lifetime of the electrons, representing the loss resulting from pitch angle diffusion. The lifetimes are taken to be 6/Kp outside plasmasphere and 10 days inside, as used by Ozeke et al. (2014). The only required boundary conditions are now the inner and outer L^* boundaries, again set at $L^* = 1$ and 5.5, respectively. As for VERB-3D, the phase space density at $L^* = 1$ is set to zero, and at $L^* = 5.5$ is set by Van Allen Probe measurements. The initial condition is again set from Van Allen Probe observations in the manner described above.

For the simulations using the D_{LL}^L parameterization for radial diffusion, we require the D_{LL}^L coefficient for $\mu <$ 400 MeV/G, owing to described grid setup for VERB. Liu et al. (2016) caution using D_{LL}^L for $\mu <$ 400 MeV/G, as they found that the D_{LL} data showed less agreement with their parameterization over this μ range. Here, we have therefore elected to use the D_{LL}^L value at $\mu = 400$ MeV/G for $\mu < 400$ MeV/G, effectively holding D_{LL}^L constant with μ for $\mu < 400$ MeV/G. In section 4.2, we discuss the impact of this choice further and explore various other approaches.

2.3 Normalized difference

To quantify the agreement between model output and Van Allen Probes observations, we use the normalized difference (ND) of the electron flux (j):

$$ND(L^*,t) = \frac{j_{obs}(L^*,t) - j_{model}(L^*,t)}{\max\limits_{over\ L^*\ at\ const\ t} \frac{j_{obj}(L^*,t)+j_{model}(L^*,t)}{2}} \tag{20}$$

This metric has been used previously by Subbotin and Shprits (2009) and Drozdov et al. (2017) and provides the difference between observations (j_{obs}) and model output (j_{model}) at a particular energy, L^*, α_{eq}, and time. The result is normalized by the maximum flux in the heart of the belt and is therefore particularly useful to determine how well the simulation reproduces the observed flux peaks, as well as the behavior around the maximum. To compute the normalized difference, the Van Allen Probes data is averaged over a 12-hour period and binned by L^* in steps of 0.1 L^*.

3 Modeling and comparison with observation

3.1 1-D simulations with realistic boundary conditions

Figure 2 shows 1.04 MeV, $\alpha_{eq} = 70^o$ MagEIS observations (panel a) alongside the corresponding output from four 1-D simulations with data-driven boundary conditions, each using different D_{LL} coefficients (panels b, d, f, h, g). Normalized differences between each simulation and the observations are also included (c, e, g, i), and the absolute mean of the normalized difference shown on each plot for reference. As seen in Figure 2j, the one year period covers various Kp-index levels, incorporating a range of geomagnetic changes.

For all of the 1-D VERB simulations, the model flux is generally lower than the observations for much of the outer radiation belt (the normalized difference is primar-

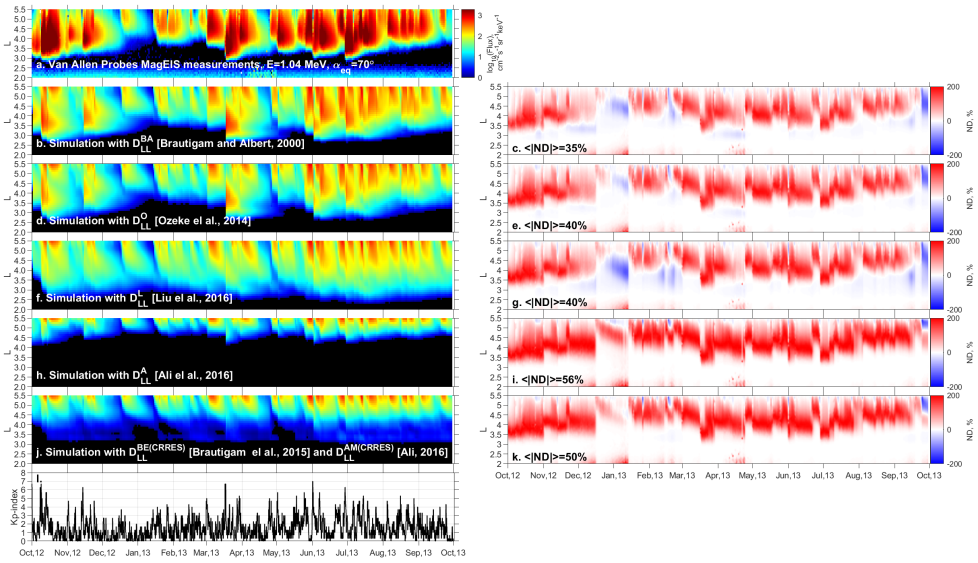

Figure 2. (a) Measurements of electron flux at 1.04 MeV, at pitch angle $\alpha = 70^\circ$ from Van Allen Probes MagEIS instrument; (b, d, f, h, j) 1-D VERB code simulation with $(D_{LL}^{BA}, D_{LL}^{O}, D_{LL}^{A}, D_{LL}^{L})$, and $D_{LL}^{BE(CRRES)} + D_{LL}^{AM(CRRES)}$ respectively; (c,e,g,i,k) normalized difference between simulations and measurements, corresponding with the mean absolute value. (l) Kp-index.

ily red). We attribute this to the absence of local acceleration from chorus waves, which has been shown to largely impact the dynamics of the ∼1 MeV population (e.g., Thorne et al., 2013; Horne et al., 2005). Although the peaks in flux are lower than the Van Allen Probes measurements, the evolution of the outer radiation belt structure is well captured when using the D_{LL}^{BA}, D_{LL}^{O} and D_{LL}^{L} coefficients. In particular, the L^* location of the inner edge of the outer belt shows closest agreement with data when using the D_{LL}^{BA} or D_{LL}^{O} coefficients. Although the D_{LL}^{BA} and D_{LL}^{O} values differ (see Figure 1), they produce very similar results in the 1-D radiation belt model.

In contrast, when using the D_{LL}^{A} coefficient, VERB-1D shows a lower flux at 1.04 MeV than observed. From examination of Figure 1, it can be seen that the electric component of D_{LL}^{A} is lower than the equivalent electric component from either D_{LL}^{O} or D_{LL}^{L} for both Kp = 1 and Kp = 5. This variation yields largely different behavior to the other three VERB-1D runs, with the outer radiation belt remaining at $L^* > 4$ for the entirety of the October 2012 to October 2013 period.

The final VERB-1D simulation, shown in Figure 2j, uses both the Ali (2016) and Brautigam et al. (2005) parameterizations. In doing so, D_{LL} coefficients are provided that are built solely on CRRES measurements, taken during the previous solar cycle. However, Ali (2016) follows the Fei et al. (2006) formalism, and accounts for only the magnetic component of the ULF wave field, while Brautigam et al. (2005) provides the radial diffusion coefficient arising from electrostatic fluctuations. As a result, the electric component of the ULF waves is not explicitly included; however, ULF wave electric fields may be partially counted in the power spectral density measurements utilized by Brautigam et al. (2005) when deriving their electrostatic diffusion coefficients. A comparison between the model output, shown in panel j, and the Van Allen Probes observations reveals a larger underestimation in the 1 MeV electron flux than when the D_{LL}^{BA}, D_{LL}^{O} and D_{LL}^{L} coefficients were used. The missing ULF wave electric component may help account for this discrepancy.

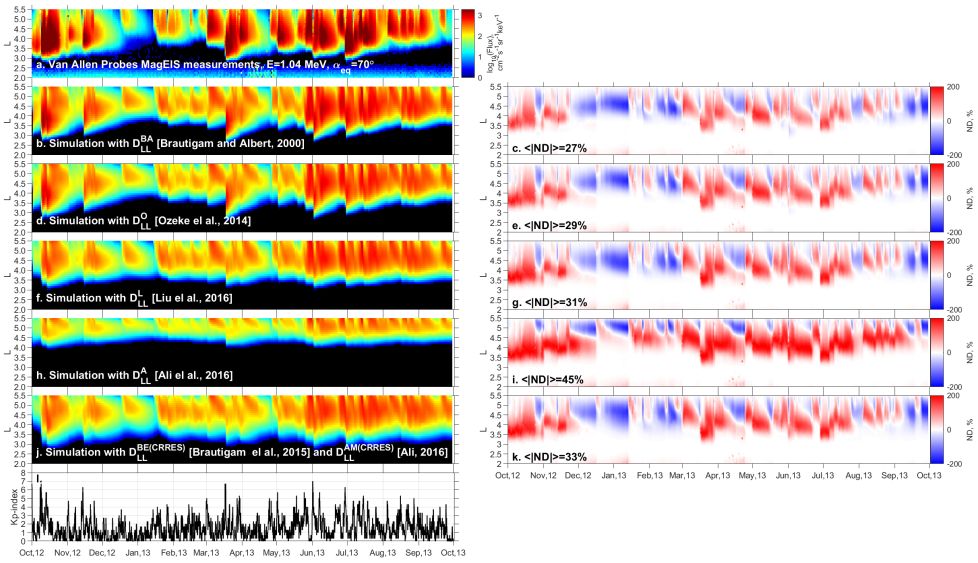

Figure 3. (a) Measurements of electron flux at 1.04 MeV, at pitch angle $\alpha = 70^\circ$ from Van Allen Probes MagEIS instrument; (b, d, f, h, j) 3-D VERB code simulation with $(D_{LL}^{BA}, D_{LL}^{O}, D_{LL}^{A}, D_{LL}^{L})$, and $D_{LL}^{BE(CRRES)} + D_{LL}^{AM(CRRES)}$ respectively; (c,e,g,i,k) normalized difference between simulations and measurements, and corresponding to the mean absolute value. (l) Kp-index.

3.2 3-D simulations including local diffusion processes

Local acceleration from chorus waves can act to produce larger flux enhancements and, as discussed in the previous section, the absence of this process is likely responsible for the lower 1 MeV flux from VERB-1D than observed. However, as the direction of radial diffusion and, in part, the rate of diffusion, are governed by the gradients in phase space density, to which local acceleration and scattering contribute, it is important to include these processes when evaluating the various radial diffusion coefficients. In this section, we use VERB-3D and include local diffusion processes as described in section 2.2.

Figure 3 takes the same format as Figure 2. The VERB-3D simulations for 1.04 MeV, $\alpha_{eq} = 70^o$, using each of the four radial diffusion coefficients, are shown (panels b, d, f, h, and j). Alongside each run, the respective normalized difference between the model output and MagEIS observations has again been included (panels c, e, f, g, and k) and the absolute mean of the normalised difference is stated on each plot. In general, electron flux levels are higher for the VERB-3D runs than VERB-1D and show closer agreement with observations. Overall, the introduction of the local processes into the simulation provides better agreement with the observations, and the improvement does not strongly depend on the selection of the radial diffusion coefficient model. This happens because of the feedback between the whistler waves induced changes (additional acceleration and loss mechanisms) and radial transport that minimize the resulting differences in the VERB code solution.

There is a tendency for the over- or underestimations of each of the model runs to occur across the same periods, albeit covering different L^* ranges. For example, regardless of the radial diffusion parameterization used, the model tends to overestimate the 1 MeV flux (for at least part of the outer radiation belt) between December 2012 and January 2013. Despite the over- and underestimations of the flux, when using $D_{LL}^{BA}, D_{LL}^{O},$,

D_{LL}^{L}, or $D_{LL}^{BE(CRRES)}$+$D_{LL}^{AM(CRRES)}$, the structure of the outer radiation belt has been generally reproduced. In particular, as was the case in the 1-D simulations, the L^* extent of the outer belt largely agrees with observations for the runs using D_{LL}^{BA} or D_{LL}^{O}. The inclusion of energy and pitch angle scattering has reduced the model flux in the observed slot region and, as a result, the inner edge of the outer belt in the 3-D model run using D_{LL}^{L} shows a closer match with observations than the corresponding output from VERB-1D. Generally, radial diffusion smooth out peaks in phase space density created by energy diffusion. Hence, the reduction of radial diffusion would cause enhance of energy diffusion while increase of the of radial diffusion will lead an increase of loss to the atmosphere (Shprits et al., 2008). This feedback mechanism can explain the why VERB-3D simulations can reproduce long-term dynamics of the radiation belts even if radial diffusion processes are quantified differently.

However, as was the case in Figure 2, the simulation with D_{LL}^{A} significantly underestimates the observed fluxes for $L^* < 4$. Although, the modelled flux is now higher than the 1-D case, the MagEIS flux is still higher than the model output. The inclusion of locally produced peaks in phase space density aids the simulation using D_{LL}^{A}; however, the additional diffusion is not sufficient to fully reproduce the radiation belt dynamics.

4 Discussion

4.1 Underestimation with D_{LL}^{A}

Our simulation results suggest that using D_{LL}^{A} in either VERB-1D or VERB-3D for the selected period significantly underestimates the observations due to insufficient radial diffusion. This parameterization employs the most recent Van Allen Probes observations. The Van Allen Probes mission has covered a relatively inactive period, with few large storms. Perhaps, as a result, the statistics for each Kp level are biased towards lower ULF wave activity. Additionally, it is the only radial diffusion coefficient used here which is only constructed for Kp < 5. The other radial diffusion parameterizations are defined up to at least Kp $= 6$. During quieter periods, radial diffusion rates are slower, and large changes in the L^* value of electron populations are generally achieved during storm periods (e.g., Ukhorskiy et al., 2009; Li et al., 2016b; Jaynes et al., 2018). Underestimating the contribution of radial diffusion during high-Kp periods is therefore likely to also impact the difference between model and observations in the following quieter times.

Another possible reason for their lower radial diffusion rates is that Ali et al. (2016) used the geometric mean (which in their case is close to the median value) of power spectral density for both electric and magnetic field spectra (see Figure 2, Ali et al., 2016). This choice was made due to the nature of the data, since the mean value of power spectral density does not represent the central tendency in the log-normal distribution that characterizes ULF power spectral density distributions. An arithmetic mean (i.e. average) of a log-normal distribution, as was used by Ozeke et al. (2014) and Liu et al. (2016), will tend to overestimate the true central tendency. However, the influence of ULF waves on electrons usually considered as the averaged effect of the wave-particle interaction. Also, radial diffusion coefficient is lineally dependent on power spectral density (e.g., equation 12). In an attempt to reproduce how the radial diffusion coefficient would have appeared if the mean of the power spectral density had instead been used, we employ a scaling factor. This approach is used purely as an illustrative estimate. The ratio between mean and median values presented in Figure 2 from Ali et al. (2016) is obtained. Since the ratio between mean and median power spectral density varies over frequency, we simplify the factor by taking the average or maximum values of the ratio. The average ($\text{factor}_{\text{mean}}$) and maximum ($\text{factor}_{\text{max}}$) values of the ratio are 3.8 and 5.0 for electric field spectra and 3.1 and 5.3 for magnetic field spectra, respectively.

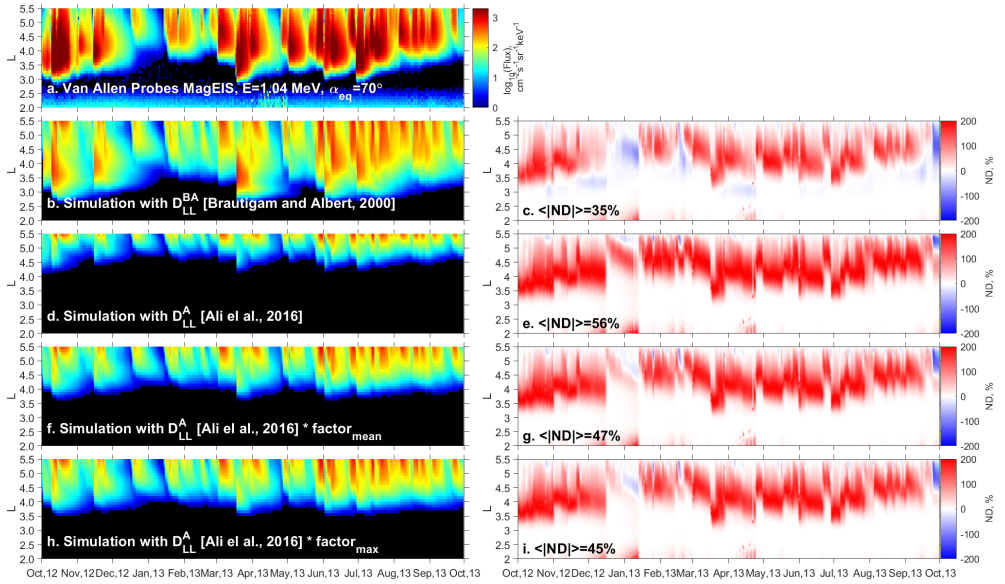

534 **Figure 4.** (a) Measurements of electron flux at 1.04 MeV, at pitch angle $\alpha = 70°$
535 from Van Allen Probes MagEIS instrument; (b, d, f, h) 1-D VERB code simulation with
536 $(D_{LL}^{BA}, D_{LL}^{A}, D_{LL}^{A}\cdot\text{factor}_{\text{mean}}, D_{LL}^{A}\cdot\text{factor}_{\text{mean}})$ respectively; (c,e,g,i) normalized difference between
537 simulations and measurements, and corresponded the mean absolute value.

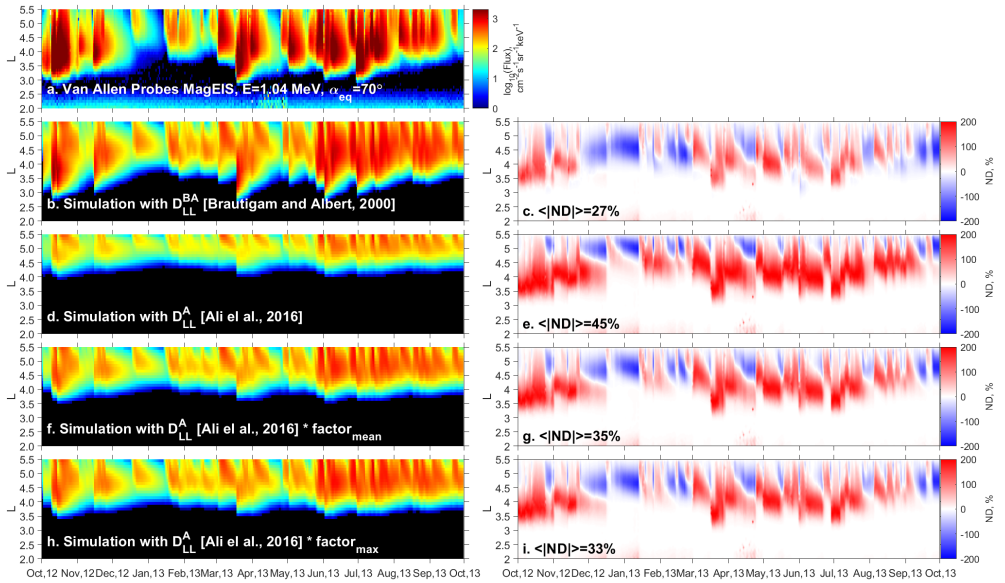

538 **Figure 5.** (a) Measurements of electron flux at 1.04 MeV, at pitch angle $\alpha = 70°$
539 from Van Allen Probes MagEIS instrument; (b, d, f, h) 3-D VERB code simulation with
540 $(D_{LL}^{BA}, D_{LL}^{A}, D_{LL}^{A}\cdot\text{factor}_{\text{mean}}, D_{LL}^{A}\cdot\text{factor}_{\text{mean}})$ respectively; (c,e,g,i) normalized difference between
541 simulations and measurements, and corresponded the mean absolute value.

Figures 4 and 5 show the result of 1-D and 3-D simulations with the scaled D_{LL}^{A} coefficients alongside simulations with unchanged D_{LL}^{A} and D_{LL}^{BA}, for reference. In both the 1-D and 3-D cases, the results of the simulation with a scaling factor provide better agreement with observations. The lower boundary of the radiation belt propagates further inward in comparison to the simulation with the unmodified coefficient. In 3-D simulations, the electron flux in the heart of the radiation belts ($L \sim 4-5$) is within an order of magnitude of the observations. The mean absolute value of normalized difference also indicates an improvement in the agreement with observations. These results highlight the difficulties in formulating a statistical picture of the power spectral density for calculating radial diffusion coefficients, as the power spectral density of ULF waves, similar to whistler waves (e.g., Watt et al., 2017), does not obey a Gaussian nature (Bentley et al., 2018).

To reproduce the Van Allen Probes flux observations using the unmodified D_{LL}^{A} coefficients, additional local acceleration or reduced loss is required. We have assumed here that the loss rates and the pitch angle and energy diffusion coefficients fully capture the extent of the wave-particle interactions. Changes in the rate of local acceleration and scattering alters the gradients in phase space density and therefore also impact how the electron populations diffuse across L^*. We argue that, given that the other D_{LL} parameterizations show better agreement with observations, the local wave particle interactions are adequately captured here.

Recent work by Tu et al. (2019) has used the magnetic radial diffusion from the Ali et al. (2016) parameterization, together with the electric radial diffusion coefficient from Liu et al. (2016) to study the June 2015 dropout event. However, as can be seen in Figure 1, the magnetic component of D_{LL} from Ali et al. (2016) is more than an order of magnitude less than the Liu et al. (2016) electric diffusion coefficient. Therefore, the evolution of the radial structure of radiation belt is largely dominated by the Liu et al. (2016) D_{LL} alone. Tu et al. (2019) also compared to model results achieved using the Brautigam and Albert (2000) D_{LL} coefficient for this event and observed differences between the two simulation outputs, with the results from the combined D_{LL}^{L} and D_{LL}^{AM} showing closer agreement with measurements. Their simulations used a larger value of L_{max}^{*} than those shown in this paper, as they did not use a data-driven outer boundary condition. Including a broader L^* range in the model may also alter how the outputs using the different D_{LL} coefficients compare to one another, as each parameterization varies across L^* differently (see Figure 1). One should also be mindful of the L^* (or L) range over which the diffusion coefficient is defined.

4.2 "Energy" dependence of D_{LL}^{L}

As discussed in section 1.1, the Liu et al. (2016) electric parameterization and Brautigam et al. (2005) electic parameterization include a μ dependence. In the other studies, the μ dependence of the electric component of D_{LL} has not been included, as the drift-averaged power spectral density of the ULF waves was taken to be frequency-independent. In the case of the Brautigam and Albert (2000) coefficient, we have neglected the electrostatic term containing μ.

Liu et al. (2016) found that the root-mean-square errors of their fitted D_{LL} increased substantially for $\mu <$ 400 MeV/G and, as a result, use of the resulting D_{LL}^{L} coefficients is therefore cautioned for $\mu <$ 400 MeV/G. Given the model grid used for VERB-3D, we require D_{LL} values for $\mu <$ 400 MeV/G and, as described in section 2.2, for the results shown in sections 3.1 and 3.2, we therefore elected to hold the D_{LL} value constant with $\mu =$ 400 MeV/G for $\mu <$ 400 MeV/G. However, an alternative approach is to allow the D_{LL}^{L} to obey the given μ dependence regardless of the μ value, ignoring the caution given. Figure 6b shows the result of this approach.

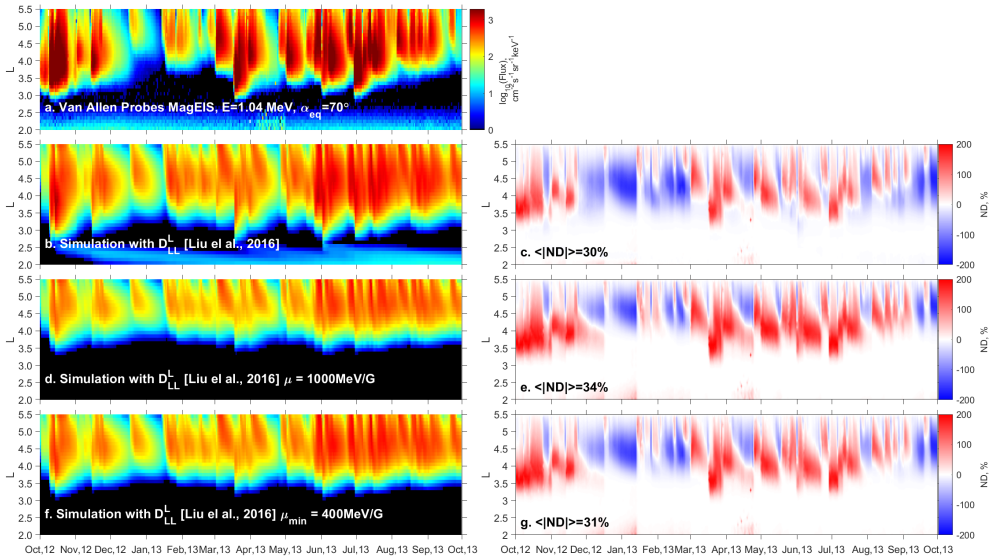

Figure 6. (a) Measurements of electron flux at 1.04 MeV, at pitch angle $\alpha = 70°$ from Van Allen Probes MagEIS instrument. (b) 3-D simulation with $D_{LL}^{L}(Kp, \mu)$, (d) with $D_{LL}^{L}(kp, \mu_0)$, where $\mu_0 = 1000\ MeV/G$, (f) with $D_{LL}^{L}(kp, \mu_{min})$, where $\mu_{min} \geq 400\ MeV/G$. (c, e, g) Normalized difference between simulations on panels (c, d, f) and measurements, and corresponding to the mean absolute value

In contrast with the results from holding D_{LL}^{L} constant with μ for $\mu <$ 400 MeV/G (also shown in Figure 6f), the VERB-3D simulation using the unlimited D_{LL}^{L} produces higher flux peaks for $L^* \sim 4$ and, from considering the normalized difference (Figure 6c), we see that these peaks are closer to the observed flux levels. Additionally, a remnant belt between $2 < L^* < 2.5$ has also been produced that is not observed by Van Allen Probe. Overestimations of the electron flux now extend over a broader L^* range than previously. Regardless, the mean absolute normalized difference is still marginally smaller (~ 1 %) than the case when D_{LL}^{L} was limited for $\mu <$ 400 MeV/G.

Another approach is to ignore the μ dependence of D_{LL}^{L} entirely, and therefore bring the parameterization in line with the other radial diffusion coefficients considered in this paper. Here, we also explore this with the 3-D model. D_{LL}^{L} is set by $\mu = 1000$ MeV/G and then assumed to be μ-independent. Figure 6d shows the resulting flux at 1.04 MeV, $\alpha_{eq} = 70^o$. The modelled flux is lower than the output shown in both Figures 6b and 6f, and the outer radiation belt extends over a smaller L^* range. Examination of the normalized difference (Figure 6e) reveals larger underestimations in comparison to data.

Including the μ dependence of D_{LL}^{L} improves the agreement between the VERB model output and observations. However, we reiterate the point made by Liu et al. (2016), that the D_{LL}^{L} for $\mu <$ 400 MeV/G should be handled carefully, as our simulations show that this can significantly impact the model output, resulting in larger flux values and a remnant belt structure.

5 Conclusions

In this study, we have used several available D_{LL} parameterizations (Brautigam & Albert, 2000; Brautigam et al., 2005; Ozeke et al., 2014; Liu et al., 2016; Ali et al., 2016; Ali, 2016), in both 1-D and 3-D radiation belt modeling, considering the same one-

year period. The simulation results have been compared, both to one another, and to observations. Our key findings are as follows:

- The difference between simulations with $D_{LL}^{BA}, D_{LL}^{O}, D_{LL}^{L}, D_{LL}^{BE(CRRES)}+D_{LL}^{AM(CRRES)}$ parameterizations is small. We suggest that the output from radiation belt models using any of these parameterizations will likely show a similar L^* structure to observations.
- 3-D simulations are observed to be less sensitive to the assumed parameterization of the radial diffusion rates than 1-D simulations.
- Simulations using D_{LL}^{A} showed 1 MeV flux levels significantly lower than observations with an outer radiation belt that did not extend below $L^* < 4$.
- The simulation with μ-dependent D_{LL}^{L}, not limited to $\mu \geq 400$ MeV/G, resulted in larger flux peaks that show better agreement with observations, but also produced a remnant belt between $2 < L^* < 2.5$, that is absent in the measurements. Ignoring the μ dependence of the Liu et al. (2016) coefficients (assuming the value corresponding to $\mu = 1000\ MeV/G$ for all μ) yielded less inwards diffusion overall and reduced the agreement with MagEIS flux values.
- The mean absolute value of the normalized difference suggests that 3-D simulations using the Brautigam and Albert (2000) coefficients (D_{LL}^{BA}) provide the best agreement with observations ($\langle|ND|\rangle = 27\%$). However, this value was comparable to that achieved in the model runs using the Ozeke et al. (2014) and Liu et al. (2016) parameterizations, which showed $\langle|ND|\rangle = 29\%$, $\langle|ND|\rangle = 31\%$ respectively. The simulation using both the parameterization from CRRES era (Brautigam et al., 2005; Ali, 2016) also gave a similar mean absolute value of the normalized difference ($\langle|ND|\rangle = 33\%$).

A clear understanding of how various radial diffusion coefficients perform is vital, both from a modelling standpoint, but additionally for understanding the impact of using different formalisms, such as an electromagnetic diffusion coefficient, separate electric and magnetic components, or neglecting the magnetic component altogether (e.g., Fei et al., 2006; Brautigam & Albert, 2000). Further improvement of the simulation results would require an improvement in understanding of the radial diffusion and more accurate quantification of the radial diffusion. We suggest that, as new parameterizations for radial diffusion coefficients are developed, they should also be bench-marked against pre-existing values to monitor progression in performance.

Acknowledgments

The authors used geomagnetic indices provided by OMNIWeb (`https://omniweb.gsfc.nasa.gov/`) and are grateful to the RBSP-ECT team for the provision of Van Allen Probes observations (`https://rbsp-ect.lanl.gov/`). The data to reproduce the figures is available at UCLA dataverse repository (`https://doi.org/10.25346/S6/U9WFPD`). This research is supported by NASA awards 80NSSC18K0663. We would like to thank Dmitry Subbotin, Ksenia Orlova, Hui Zhu, Dedong Wang, Adam Kellerman and Geoff Reeves for useful discussions. This work used computational and storage services associated with the Hoffman2 Shared Cluster provided by UCLA Institute for Digital Research and Educations Research Technology Group. The authors also acknowledge the developers of the International Radiation Belt Environment Modeling (IRBEM) library.

References

Ali, A. F. (2016). *ULF waves and diffusive radial transport of charged particles* (Unpublished doctoral dissertation). Faculty of the Graduate School of the University of Colorado.

Ali, A. F., Elkington, S. R., Tu, W., Ozeke, L. G., Chan, A. A., & Friedel, R. H. W.

(2015, February). Magnetic field power spectra and magnetic radial diffusion coefficients using CRRES magnetometer data. *J. Geophys. Res. [Space Phys]*, *120*(2), 973–995. doi: 10.1002/2014JA020419

Ali, A. F., Malaspina, D. M., Elkington, S. R., Jaynes, A. N., Chan, A. A., Wygant, J., & Kletzing, C. A. (2016, October). Electric and magnetic radial diffusion coefficients using the van allen probes data. *J. Geophys. Res. [Space Phys]*, *121*(10), 2016JA023002. doi: 10.1002/2016JA023002

Baker, D. N., Kanekal, S. G., Hoxie, V. C., Batiste, S., Bolton, M., Li, X., ... Friedel, R. (2013, November). The relativistic Electron-Proton telescope (REPT) instrument on board the radiation belt storm probes (RBSP) spacecraft: Characterization of earth's radiation belt High-Energy particle populations. *Space Sci. Rev.*, *179*(1-4), 337–381. doi: 10.1007/s11214-012-9950-9

Barani, M., Tu, W., Sarris, T., Pham, K., & Redmon, R. J. (2019, July). Estimating the azimuthal mode structure of ULF waves based on multiple GOES satellite observations. *J. Geophys. Res. [Space Phys]*, *124*(7), 5009–5026. doi: 10.1029/2019JA026927

Bentley, S. N., Watt, C. E. J., Owens, M. J., & Rae, I. J. (2018). Ulf wave activity in the magnetosphere: Resolving solar wind interdependencies to identify driving mechanisms. *Journal of Geophysical Research: Space Physics*, *123*(4), 2745-2771. Retrieved from `https://agupubs.onlinelibrary.wiley.com/doi/abs/10.1002/2017JA024740` doi: 10.1002/2017JA024740

Blake, J. B., Carranza, P. A., Claudepierre, S. G., Clemmons, J. H., Crain, W. R., Jr., Dotan, Y., ... Zakrzewski, M. P. (2013, November). The magnetic electron ion spectrometer (MagEIS) instruments aboard the radiation belt storm probes (RBSP) spacecraft. *Space Sci. Rev.*, *179*(1-4), 383–421. doi: 10.1007/s11214-013-9991-8

Brautigam, D. H., & Albert, J. M. (2000). Radial diffusion analysis of outer radiation belt electrons during the october 9, 1990, magnetic storm. *J. Geophys. Res.*, *105*(A1), 291–309. doi: 10.1029/1999ja900344

Brautigam, D. H., Ginet, G. P., Albert, J. M., Wygant, J. R., Rowland, D. E., Ling, A., & Bass, J. (2005). CRRES electric field power spectra and radial diffusion coefficients. *J. Geophys. Res.*, *110*(A2), 10,495. doi: 10.1029/2004JA010612

Brizard, A. J., & Chan, A. A. (2001). Relativistic bounce-averaged quasilinear diffusion equation for low-frequency electromagnetic fluctuations. *Physics of Plasmas*, *8*(11), 4762-4771. Retrieved from `https://doi.org/10.1063/1.1408623` doi: 10.1063/1.1408623

Califf, S., & Cully, C. M. (2016, July). Empirical estimates and theoretical predictions of the shorting factor for the THEMIS double-probe electric field instrument: THEMIS shorting factor. *J. Geophys. Res. [Space Phys]*, *121*(7), 6223–6233. doi: 10.1002/2016JA022589

Califf, S., Li, X., Blum, L., Jaynes, A., Schiller, Q., Zhao, H., ... Bonnell, J. W. (2014, December). THEMIS measurements of quasi-static electric fields in the inner magnetosphere. *J. Geophys. Res. [Space Phys]*, *119*(12), 9939–9951. doi: 10.1002/2014JA020360

Cornwall, J. M. (1968). Diffusion processes influenced by conjugate-point wave phenomena. *Radio Sci.*, *3*(7), 740–744.

Drozdov, A. Y., Shprits, Y. Y., Aseev, N. A., Kellerman, A. C., & Reeves, G. D. (2017). Dependence of radiation belt simulations to assumed radial diffusion rates tested for two empirical models of radial transport. *Space Weather*, *15*(1), 2016SW001426. doi: 10.1002/2016SW001426

Elkington, S. R., Chan, A. A., & Wiltberger, M. (2012, January). Global structure of ULF waves during the 24-26 september 1998 geomagnetic storm: Summers/Dynamics of the earth's radiation belts and inner magnetosphere. In D. Summers, I. R. Mann, D. N. Baker, & M. Schulz (Eds.), *Dynamics of the earth's radiation belts and inner magnetosphere* (Vol. 169, pp. 127–138). Wash-

ington, D. C.: American Geophysical Union. doi: 10.1029/2012GM001348

Elkington, S. R., Hudson, M. K., & Chan, A. A. (1999). Acceleration of relativistic electrons via drift-resonant interaction with toroidal-mode pc-5 ulf oscillations. *Geophysical Research Letters*, *26*(21), 3273-3276. Retrieved from https://agupubs.onlinelibrary.wiley.com/doi/abs/10.1029/1999GL003659 doi: 10.1029/1999GL003659

Elkington, S. R., Hudson, M. K., & Chan, A. A. (2003). Resonant acceleration and diffusion of outer zone electrons in an asymmetric geomagnetic field. *J. Geophys. Res. [Space Phys]*, *108*(A3). doi: 10.1029/2001JA009202

Fälthammar, C. G. (1968). Radial diffusion by violation of the third adiabatic invariant, earth's particles and fields. In B. M. McCormac (Ed.), *Earth's particles and fields* (Vol. 157, pp. 157–169). New York: Reinhold.

Fei, Y., Chan, A. A., Elkington, S. R., & Wiltberger, M. J. (2006). Radial diffusion and mhd particle simulations of relativistic electron transport by ulf waves in the september 1998 storm. *Journal of Geophysical Research: Space Physics*, *111*(A12). Retrieved from https://agupubs.onlinelibrary.wiley.com/doi/abs/10.1029/2005JA011211 doi: 10.1029/2005JA011211

Flthammar, C.-G. (1965). Effects of time-dependent electric fields on geomagnetically trapped radiation. *Journal of Geophysical Research (1896-1977)*, *70*(11), 2503-2516. Retrieved from https://agupubs.onlinelibrary.wiley.com/doi/abs/10.1029/JZ070i011p02503 doi: 10.1029/JZ070i011p02503

Glauert, S. A., Horne, R. B., & Meredith, N. P. (2014). Simulating the earth's radiation belts: internal acceleration and continuous losses to the magnetopause. *J. Geophys. Res. [Space Phys]*. doi: 10.1002/2014JA020092

Holzworth, R. H., & Mozer, F. S. (1979). Direct evaluation of the radial diffusion coefficient near l=6 due to electric field fluctuations. *J. Geophys. Res.*, *84*(A6), 2559. doi: 10.1029/JA084iA06p02559

Horne, R. B., Thorne, R. M., Glauert, S. A., Albert, J. M., Meredith, N. P., & Anderson, R. R. (2005). Timescale for radiation belt electron acceleration by whistler mode chorus waves. *Journal of Geophysical Research: Space Physics*, *110*(A3). Retrieved from https://agupubs.onlinelibrary.wiley.com/doi/abs/10.1029/2004JA010811 doi: 10.1029/2004JA010811

Jacobs, J. A., Kato, Y., Matsushita, S., & Troitskaya, V. A. (1964). Classification of geomagnetic micropulsations. *Journal of Geophysical Research (1896-1977)*, *69*(1), 180-181. Retrieved from https://agupubs.onlinelibrary.wiley.com/doi/abs/10.1029/JZ069i001p00180 doi: 10.1029/JZ069i001p00180

Jaynes, A. N., Ali, A. F., Elkington, S. R., Malaspina, D. M., Baker, D. N., Li, X., ... Wygant, J. R. (2018, October). Fast diffusion of ultrarelativistic electrons in the outer radiation belt: 17 march 2015 storm event. *Geophys. Res. Lett.*, *45*(20), 10874–10882. doi: 10.1029/2018GL079786

Kim, K.-C., Shprits, Y., Subbotin, D., & Ni, B. (2011). Understanding the dynamic evolution of the relativistic electron slot region including radial and pitch angle diffusion. *J. Geophys. Res. [Space Phys]*, *116*(A10). doi: 10.1029/2011JA016684

Lanzerotti, L. J., & Morgan, C. G. (1973). ULF geomagnetic power near l= 4: 2. temporal variation of the radial diffusion coefficient for relativistic electrons. *J. Geophys. Res.*.

Lejosne, S., Boscher, D., Maget, V., & Rolland, G. (2013). Deriving electromagnetic radial diffusion coefficients of radiation belt equatorial particles for different levels of magnetic activity based on magnetic field measurements at geostationary orbit. *Journal of Geophysical Research: Space Physics*, *118*(6), 3147-3156. Retrieved from https://agupubs.onlinelibrary.wiley.com/doi/abs/10.1002/jgra.50361 doi: 10.1002/jgra.50361

Lejosne, S., & Kollmann, P. (2019). Radiation belt radial diffusion at earth and beyond. *Earth and Space Science Open Archive*. doi: 10.1002/essoar.10501074.1

Li, Z., Hudson, M., Paral, J., Wiltberger, M., & Turner, D. (2016a, July). Global ULF wave analysis of radial diffusion coefficients using a global MHD model for the 17 march 2015 storm: RADIAL DIFFUSION COEFFICIENT CALCULATION. *J. Geophys. Res. [Space Phys]*, *121*(7), 6196–6206. doi: 10.1002/2016JA022508

Li, Z., Hudson, M., Paral, J., Wiltberger, M., & Turner, D. (2016b, July). Global ULF wave analysis of radial diffusion coefficients using a global MHD model for the 17 march 2015 storm: RADIAL DIFFUSION COEFFICIENT CALCULATION. *J. Geophys. Res. [Space Phys]*, *121*(7), 6196–6206. doi: 10.1002/2016JA022508

Li, Z., Hudson, M., Patel, M., Wiltberger, M., Boyd, A., & Turner, D. (2017, July). ULF wave analysis and radial diffusion calculation using a global MHD model for the 17 march 2013 and 2015 storms. *J. Geophys. Res. [Space Phys]*, *122*(7), 7353–7363. doi: 10.1002/2016JA023846

Liu, W., Tu, W., Li, X., Sarris, T., Khotyaintsev, Y., Fu, H., ... Shi, Q. (2016, February). On the calculation of electric diffusion coefficient of radiation belt electrons with in situ electric field measurements by THEMIS. *Geophys. Res. Lett.*, *43*(3), 2015GL067398. doi: 10.1002/2015GL067398

Mager, P. N., & Klimushkin, D. Y. (2005, December). Spatial localization and azimuthal wave numbers of alfvén waves generated by drift-bounce resonance in the magnetosphere. *Ann. Geophys.*, *23*(12), 3775–3784. doi: 10.5194/angeo-23-3775-2005

Malaspina, D. M., Claudepierre, S. G., Takahashi, K., Jaynes, A. N., Elkington, S. R., Ergun, R. E., ... Kletzing, C. A. (2015, November). Kinetic alfvén waves and particle response associated with a shock-induced, global ULF perturbation of the terrestrial magnetosphere: KAW FROM SHOCK IMPACT. *Geophys. Res. Lett.*, *42*(21), 9203–9212. doi: 10.1002/2015GL065935

McIlwain, C. E. (1961, November). Coordinates for mapping the distribution of magnetically trapped particles. *J. Geophys. Res.*, *66*(11), 3681–3691. doi: 10.1029/JZ066i011p03681

Ni, B., Thorne, R. M., Shprits, Y. Y., & Bortnik, J. (2008). Resonant scattering of plasma sheet electrons by whistler-mode chorus: Contribution to diffuse auroral precipitation. *Geophysical Research Letters*, *35*(11). Retrieved from `https://agupubs.onlinelibrary.wiley.com/doi/abs/10.1029/2008GL034032` doi: 10.1029/2008GL034032

Olifer, L., Mann, I. R., Ozeke, L. G., Rae, I. J., & Morley, S. K. (2019, April). On the relative strength of electric and magnetic ULF wave radial diffusion during the march 2015 geomagnetic storm. *J. Geophys. Res. [Space Phys]*. doi: 10.1029/2018JA026348

Orlova, K. G., & Shprits, Y. Y. (2011, September). On the bounce-averaging of scattering rates and the calculation of bounce period. *Phys. Plasmas*, *18*(9), 092904. doi: 10.1063/1.3638137

Orlova, K. G., Shprits, Y. Y., & Ni, B. (2012). Bounce-averaged diffusion coefficients due to resonant interaction of the outer radiation belt electrons with oblique chorus waves computed in a realistic magnetic field model. *J. Geophys. Res. [Space Phys]*, *117*(A7). doi: 10.1029/2012JA017591

Orlova, K. G., Spasojevic, M., & Shprits, Y. (2014). Activity-dependent global model of electron loss inside the plasmasphere. *Geophys. Res. Lett.*, *41*(11), 3744–3751. doi: 10.1002/2014GL060100

Ozeke, L. G., & Mann, I. R. (2001, August). Modeling the properties of high- m alfvén waves driven by the drift-bounce resonance mechanism. *J. Geophys. Res.*, *106*(A8), 15583–15597. doi: 10.1029/2000JA000393

Ozeke, L. G., Mann, I. R., Murphy, K. R., Jonathan Rae, I., & Milling, D. K. (2014). Analytic expressions for ULF wave radiation belt radial diffusion coefficients. *J. Geophys. Res. [Space Phys]*, *119*(3), 1587–1605. doi:

10.1002/2013JA019204

Ozeke, L. G., Mann, I. R., Murphy, K. R., Rae, I. J., Milling, D. K., Elkington, S. R., ... Singer, H. J. (2012). ULF wave derived radiation belt radial diffusion coefficients. *J. Geophys. Res. [Space Phys]*, *117*(A4). doi: 10.1029/2011JA017463

Perry, K. L., Hudson, M. K., & Elkington, S. R. (2005). Incorporating spectral characteristics of pc5 waves into three-dimensional radiation belt modeling and the diffusion of relativistic electrons. *J. Geophys. Res.*, *110*(A3), 14,853. doi: 10.1029/2004JA010760

Roederer, J. G. (1970). *Dynamics of geomagnetically trapped radiation:*. Springer Berlin Heidelberg. doi: 10.1007/978-3-642-49300-3

Sarris, T. E., Li, X., Liu, W., Argyriadis, E., Boudouridis, A., & Ergun, R. (2013, November). Mode number calculations of ULF field-line resonances using ground magnetometers and THEMIS measurements: MODE NUMBER OF ULF FIELD-LINE RESONANCES. *J. Geophys. Res. [Space Phys]*, *118*(11), 6986–6997. doi: 10.1002/2012JA018307

Schulz, M., & Eviatar, A. (1969, May). Diffusion of equatorial particles in the outer radiation zone. *J. Geophys. Res.*, *74*(9), 2182–2192. doi: 10.1029/JA074i009p02182

Schulz, M., & Lanzerotti, L. J. (1974). *Particle diffusion in the radiation belts* (Vol. 7). Springer.

Shprits, Y. Y., Elkington, S. R., Meredith, N. P., & Subbotin, D. A. (2008). Review of modeling of losses and sources of relativistic electrons in the outer radiation belt i: Radial transport. *Journal of Atmospheric and Solar-Terrestrial Physics*, *70*(14), 1679 - 1693. Retrieved from `http://www.sciencedirect.com/science/article/pii/S1364682608001648` (Dynamic Variability of Earth's Radiation Belts) doi: https://doi.org/10.1016/j.jastp.2008.06.008

Shprits, Y. Y., Kellerman, A. C., Drozdov, A. Y., Spence, H. E., Reeves, G. D., & Baker, D. N. (2015, January). Combined convective and diffusive simulations: VERB-4D comparison with 17 march 2013 van allen probes observations. *Geophys. Res. Lett.*, 2015GL065230. doi: 10.1002/2015GL065230

Shprits, Y. Y., & Ni, B. (2009). Dependence of the quasi-linear scattering rates on the wave normal distribution of chorus waves. *Journal of Geophysical Research: Space Physics*, *114*(A11). Retrieved from `https://agupubs.onlinelibrary.wiley.com/doi/abs/10.1029/2009JA014223` doi: 10.1029/2009JA014223

Shue, J.-H., Song, P., Russell, C. T., Steinberg, J. T., Chao, J. K., Zastenker, G., ... Kawano, H. (1998, August). Magnetopause location under extreme solar wind conditions. *J. Geophys. Res.*, *103*(A8), 17691–17700. doi: 10.1029/98JA01103

Stratton, J. M., Harvey, R. J., & Heyler, G. A. (2013, November). Mission overview for the radiation belt storm probes mission. *Space Sci. Rev.*, *179*(1), 29–57. doi: 10.1007/s11214-012-9933-x

Subbotin, D. A., & Shprits, Y. Y. (2009, October). Three-dimensional modeling of the radiation belts using the versatile electron radiation belt (VERB) code. *Space Weather*, *7*(10), S10001. doi: 10.1029/2008SW000452

Subbotin, D. A., & Shprits, Y. Y. (2012, May). Three-dimensional radiation belt simulations in terms of adiabatic invariants using a single numerical grid. *J. Geophys. Res.*, *117*(A5), A05205. doi: 10.1029/2011JA017467

Subbotin, D. A., Shprits, Y. Y., & Ni, B. (2011). Long-term radiation belt simulation with the VERB 3-D code: Comparison with CRRES observations. *J. Geophys. Res. [Space Phys]*, *116*(A12), A12210. doi: 10.1029/2011JA017019

Takahashi, K., & Anderson, B. J. (1992). Distribution of ULF energy (f ¡ 80 mhz) in the inner magnetosphere: A statistical analysis of AMPTE CCE magnetic field data. *J. Geophys. Res.*, *97*(A7), 10751. doi: 10.1029/92JA00328

Thorne, R. M., Li, W., Ni, B., Ma, Q., Bortnik, J., Chen, L., ... Kanekal,

S. G. (2013). Rapid local acceleration of relativistic radiation-belt electrons by magnetospheric chorus. *Nature*, *504*, 411-414. Retrieved from https://doi.org/10.1038/nature12889 doi: 10.1038/nature12889

Tsyganenko, N. A., & Sitnov, M. I. (2007, June). Magnetospheric configurations from a high-resolution data-based magnetic field model. *J. Geophys. Res.*, *112*(A6), A06225. doi: 10.1029/2007JA012260

Tu, W., Elkington, S. R., Li, X., Liu, W., & Bonnell, J. (2012, October). Quantifying radial diffusion coefficients of radiation belt electrons based on global MHD simulation and spacecraft measurements: QUANTIFY RADIAL DIFFUSION COEFFICIENTS. *J. Geophys. Res.*, *117*(A10). doi: 10.1029/2012JA017901

Tu, W., Xiang, Z., & Morley, S. K. (2019). Modeling the magnetopause shadowing loss during the june 2015 dropout event. *Geophysical Research Letters*, *46*(16), 9388-9396. Retrieved from https://agupubs.onlinelibrary.wiley.com/doi/abs/10.1029/2019GL084419 doi: 10.1029/2019GL084419

Ukhorskiy, A. Y., & Sitnov, M. I. (2013, Nov 01). Dynamics of radiation belt particles. *Space Science Reviews*, *179*(1), 545–578. Retrieved from https://doi.org/10.1007/s11214-012-9938-5 doi: 10.1007/s11214-012-9938-5

Ukhorskiy, A. Y., Sitnov, M. I., Takahashi, K., & Anderson, B. J. (2009, May). Radial transport of radiation belt electrons due to stormtime pc5 waves. *Ann. Geophys.*, *27*(5), 2173–2181. doi: 10.5194/angeo-27-2173-2009

Ukhorskiy, A. Y., Takahashi, K., Anderson, B. J., & Korth, H. (2005). Impact of toroidal ULF waves on the outer radiation belt electrons. *J. Geophys. Res.*, *110*(A10), 128. doi: 10.1029/2005JA011017

Watt, C. E. J., Rae, I. J., Murphy, K. R., Anekallu, C., Bentley, S. N., & Forsyth, C. (2017). The parameterization of wave-particle interactions in the outer radiation belt. *Journal of Geophysical Research: Space Physics*, *122*(9), 9545-9551. Retrieved from https://agupubs.onlinelibrary.wiley.com/doi/abs/10.1002/2017JA024339 doi: 10.1002/2017JA024339

Figure 1.

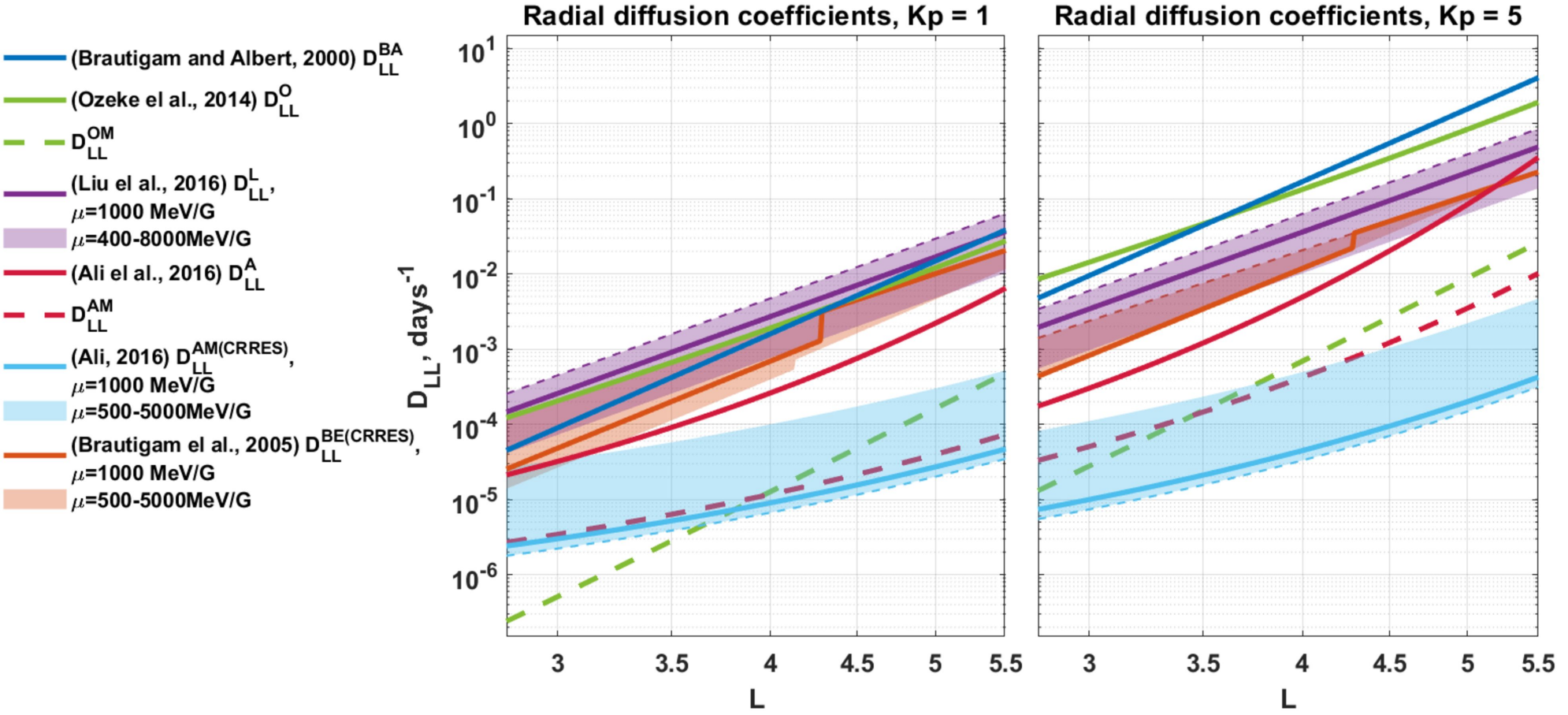
(Brautigam and Albert, 2000) D_{LL}^{BA}
(Ozeke el al., 2014) D_{LL}^{O}
D_{LL}^{OM}
(Liu el al., 2016) D_{LL}^{L},
μ=1000 MeV/G
μ=400-8000MeV/G
(Ali el al., 2016) D_{LL}^{A}
D_{LL}^{AM}
(Ali, 2016) $D_{LL}^{AM(CRRES)}$,
μ=1000 MeV/G
μ=500-5000MeV/G
(Brautigam el al., 2005) $D_{LL}^{BE(CRRES)}$,
μ=1000 MeV/G
μ=500-5000MeV/G
Radial diffusion coefficients, Kp = 1
Radial diffusion coefficients, Kp = 5
D_{LL}, days^{-1}
10^{1}
10^{0}
10^{-1}
10^{-2}
10^{-3}
10^{-4}
10^{-5}
10^{-6}
3
3.5
4
4.5
5
5.5
L

Figure 2.

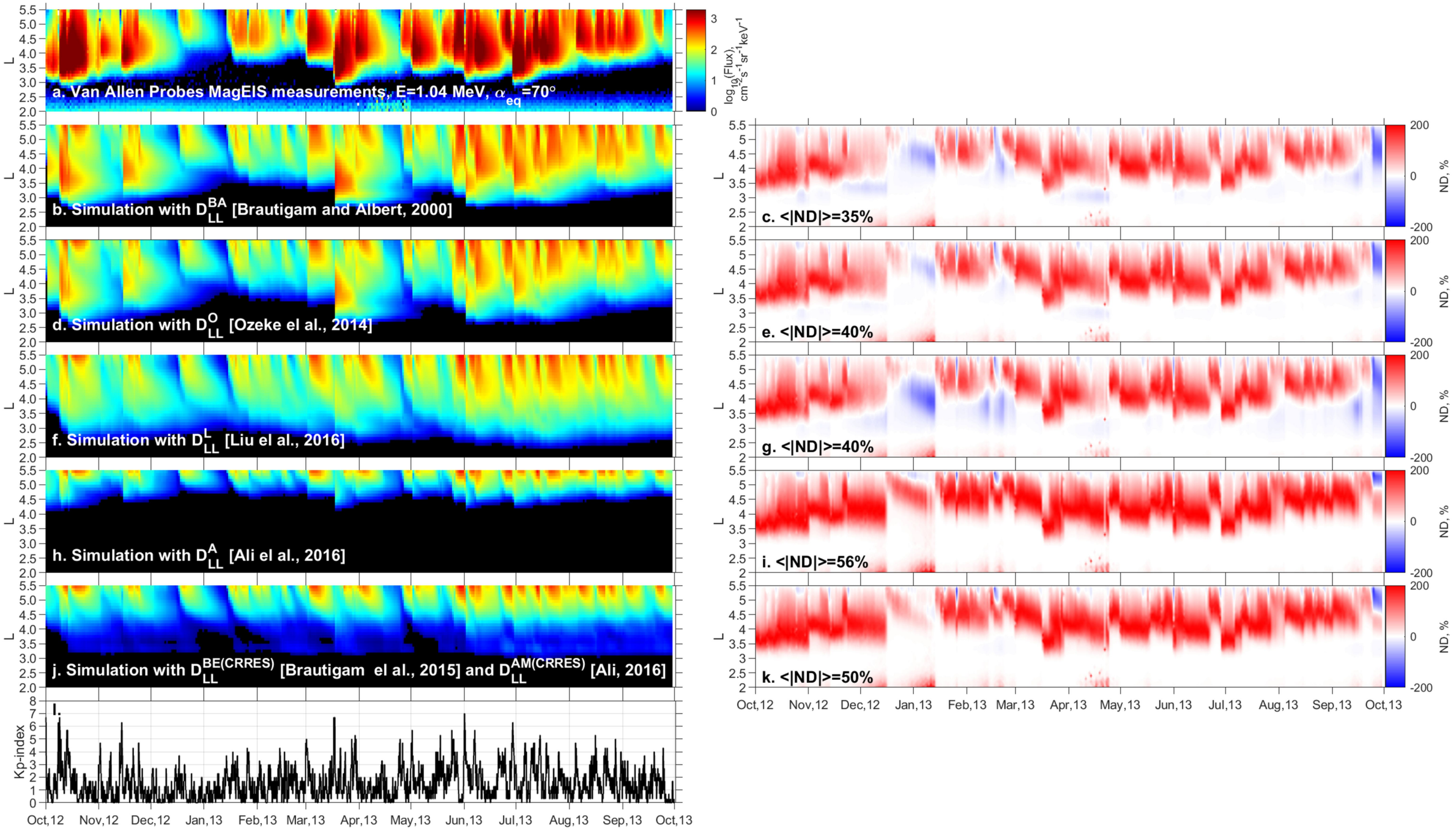
a. Van Allen Probes MagEIS measurements, E=1.04 MeV, α_{eq}=70°
b. Simulation with D_{LL}^{BA} [Brautigam and Albert, 2000]
d. Simulation with D_{LL}^{O} [Ozeke el al., 2014]
f. Simulation with D_{LL}^{L} [Liu el al., 2016]
h. Simulation with D_{LL}^{A} [Ali el al., 2016]
j. Simulation with $D_{LL}^{BE(CRRES)}$ [Brautigam el al., 2015] and $D_{LL}^{AM(CRRES)}$ [Ali, 2016]
$\log_{10}$(Flux); $cm^{-2}s^{-1}sr^{-1}keV^{-1}$
c. <|ND|>=35%
e. <|ND|>=40%
g. <|ND|>=40%
i. <|ND|>=56%
k. <|ND|>=50%
ND, %
L
l.
Kp-index
Oct,12 Nov,12 Dec,12 Jan,13 Feb,13 Mar,13 Apr,13 May,13 Jun,13 Jul,13 Aug,13 Sep,13 Oct,13

Figure 3.

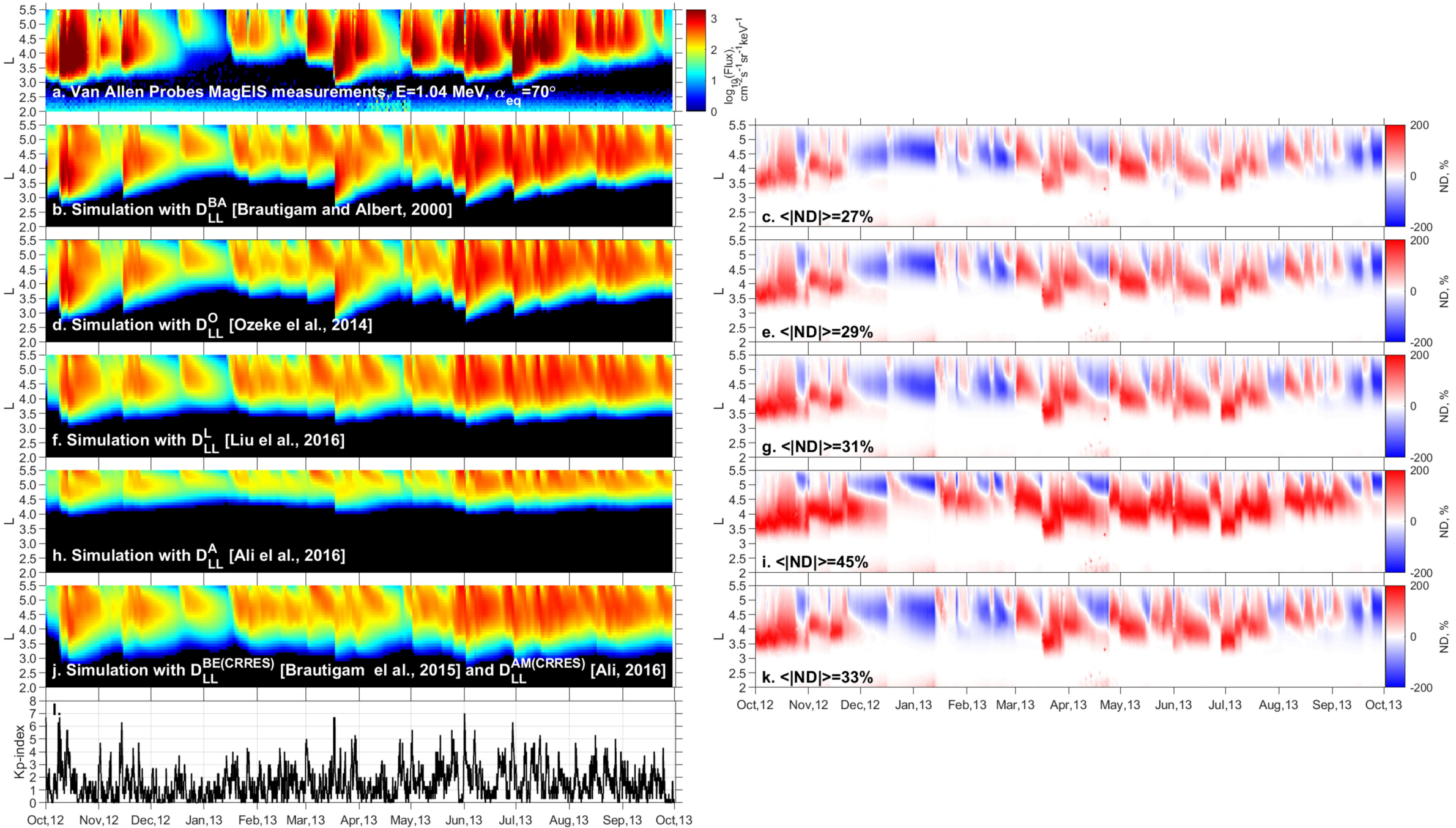
a. Van Allen Probes MagEIS measurements, E=1.04 MeV, α_{eq}=70°
b. Simulation with D_{LL}^{BA} [Brautigam and Albert, 2000]
d. Simulation with D_{LL}^{O} [Ozeke el al., 2014]
f. Simulation with D_{LL}^{L} [Liu el al., 2016]
h. Simulation with D_{LL}^{A} [Ali el al., 2016]
j. Simulation with $D_{LL}^{BE(CRRES)}$ [Brautigam el al., 2015] and $D_{LL}^{AM(CRRES)}$ [Ali, 2016]
$\log_{10}$(Flux); $cm^{-2}s^{-1}sr^{-1}keV^{-1}$
c. <|ND|>=27%
e. <|ND|>=29%
g. <|ND|>=31%
i. <|ND|>=45%
k. <|ND|>=33%
ND, %
L
l.
Kp-index
Oct,12 Nov,12 Dec,12 Jan,13 Feb,13 Mar,13 Apr,13 May,13 Jun,13 Jul,13 Aug,13 Sep,13 Oct,13

Figure 4.

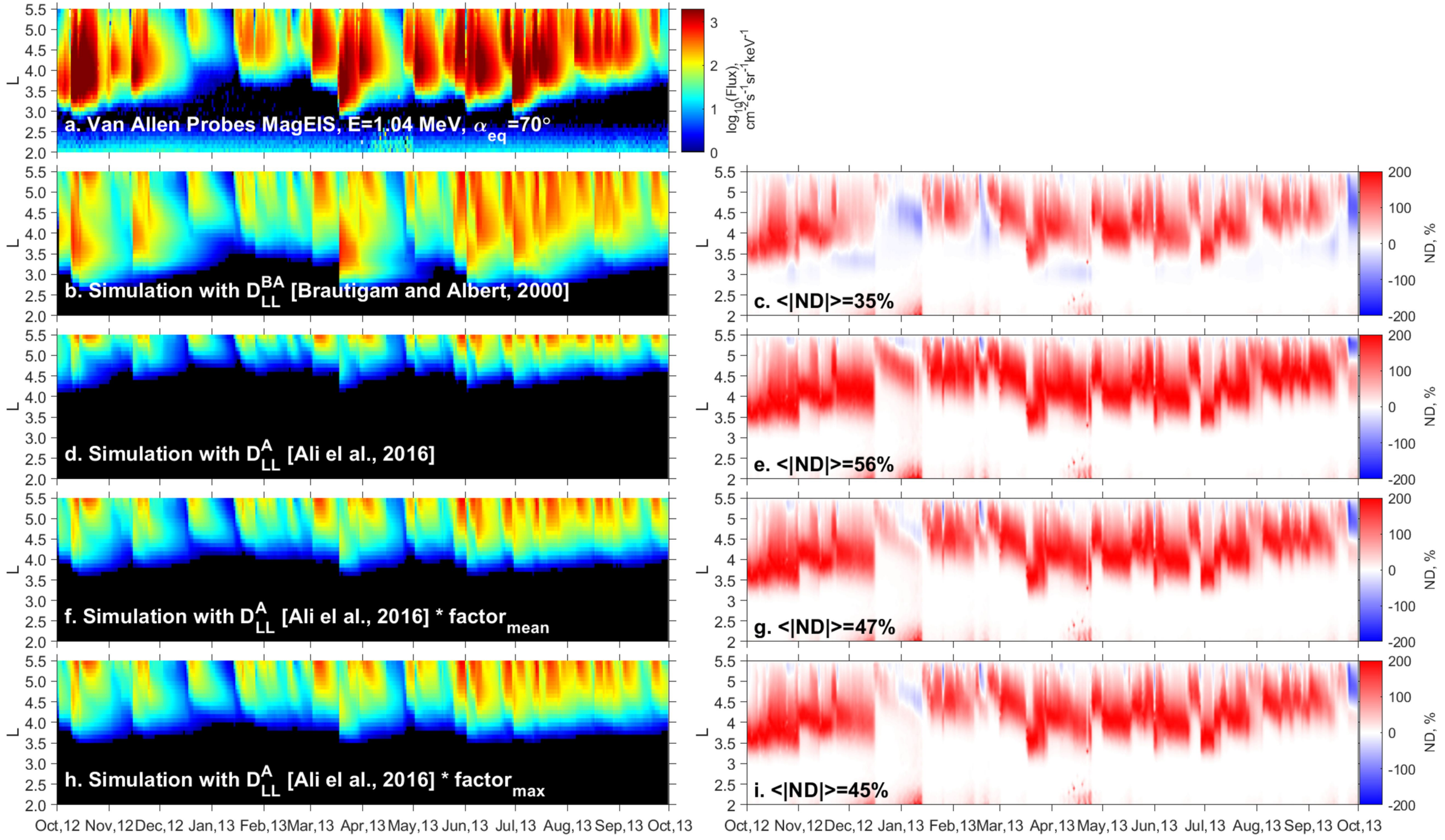
a. Van Allen Probes MagEIS, E=1.04 MeV, α_{eq}=70°
b. Simulation with D_{LL}^{BA} [Brautigam and Albert, 2000]
c. <|ND|>=35%
d. Simulation with D_{LL}^{A} [Ali el al., 2016]
e. <|ND|>=56%
f. Simulation with D_{LL}^{A} [Ali el al., 2016] * factor$_{mean}$
g. <|ND|>=47%
h. Simulation with D_{LL}^{A} [Ali el al., 2016] * factor$_{max}$
i. <|ND|>=45%
L
$\log_{10}$(Flux), cm^{-2}s^{-1}sr^{-1}keV^{-1}
ND, %
Oct,12 Nov,12 Dec,12 Jan,13 Feb,13 Mar,13 Apr,13 May,13 Jun,13 Jul,13 Aug,13 Sep,13 Oct,13

Figure 5.

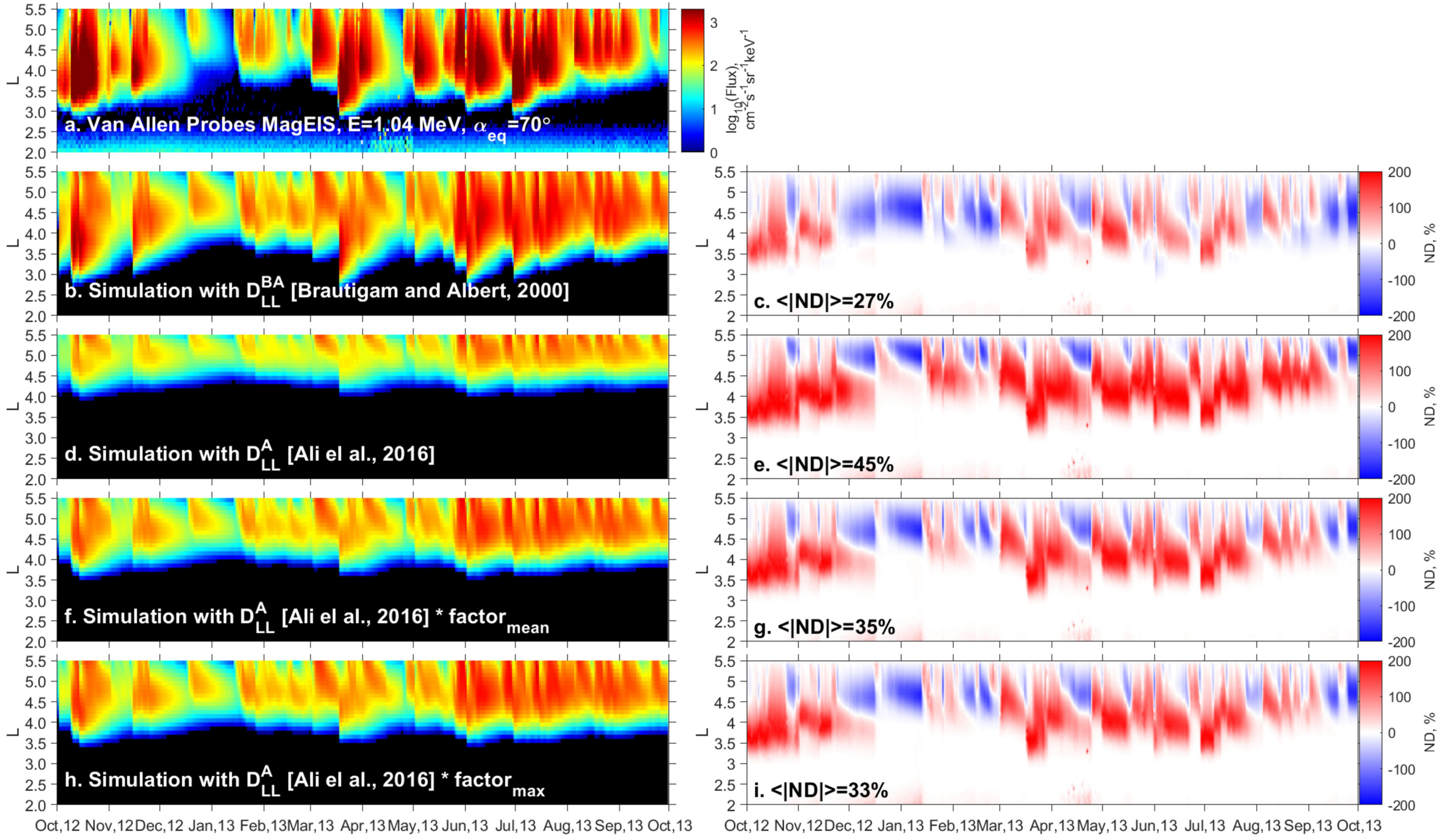
a. Van Allen Probes MagEIS, E=1.04 MeV, α_{eq}=70°
b. Simulation with D_{LL}^{BA} [Brautigam and Albert, 2000]
c. <|ND|>=27%
d. Simulation with D_{LL}^{A} [Ali el al., 2016]
e. <|ND|>=45%
f. Simulation with D_{LL}^{A} [Ali el al., 2016] * $factor_{mean}$
g. <|ND|>=35%
h. Simulation with D_{LL}^{A} [Ali el al., 2016] * $factor_{max}$
i. <|ND|>=33%
L
$\log_{10}$(Flux); $cm^{-2}s^{-1}sr^{-1}keV^{-1}$
ND, %
Oct,12 Nov,12 Dec,12 Jan,13 Feb,13 Mar,13 Apr,13 May,13 Jun,13 Jul,13 Aug,13 Sep,13 Oct,13

Figure 6.

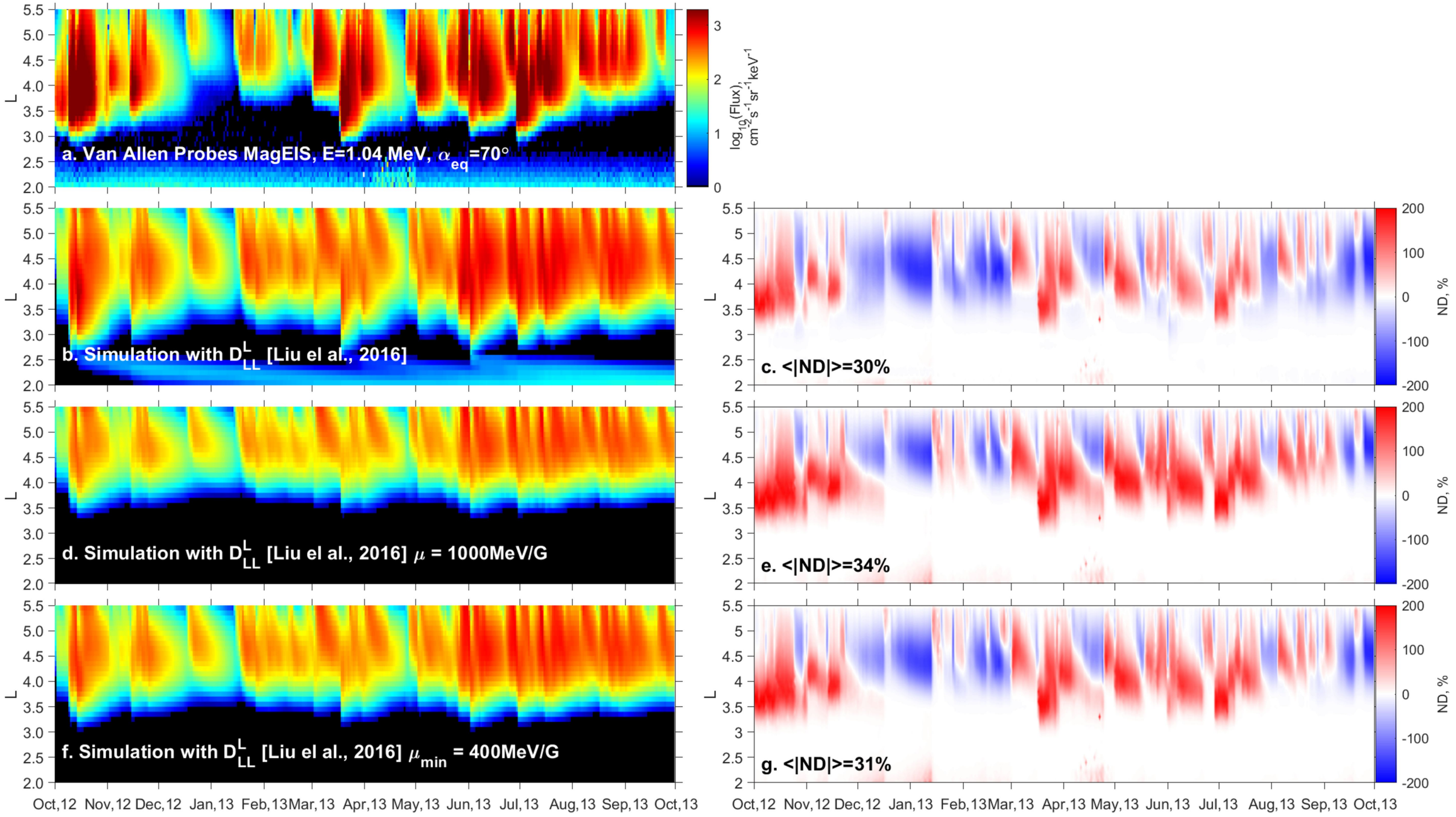
a. Van Allen Probes MagEIS, E=1.04 MeV, α_{eq}=70°
b. Simulation with D_{LL}^{L} [Liu el al., 2016]
c. <|ND|>=30%
d. Simulation with D_{LL}^{L} [Liu el al., 2016] μ = 1000MeV/G
e. <|ND|>=34%
f. Simulation with D_{LL}^{L} [Liu el al., 2016] μ_{min} = 400MeV/G
g. <|ND|>=31%
L
$\log_{10}$(Flux), $cm^{-2}s^{-1}sr^{-1}keV^{-1}$
ND, %
Oct,12 Nov,12 Dec,12 Jan,13 Feb,13 Mar,13 Apr,13 May,13 Jun,13 Jul,13 Aug,13 Sep,13 Oct,13